Natural Variation of Molecular and Morphological Gibberellin Responses[1][OPEN]

Youn-Jeong Nam[2], Dorota Herman[2], Jonas Blomme, Eunyoung Chae, Mikiko Kojima, Frederik Coppens, Veronique Storme, Twiggy Van Daele, Stijn Dhondt, Hitoshi Sakakibara, Detlef Weigel, Dirk Inzé[3]*, and Nathalie Gonzalez[2,3,4]

Department of Plant Systems Biology, VIB, B-9052 Gent, Belgium (Y.J.N., D.H., F.C., V.S., T.V.D., S.D., D.I., N.G.); Department of Plant Biotechnology and Bioinformatics, Ghent University, B-9052 Gent, Belgium (Y.J.N., D.H., F.C., V.S., T.V.D., S.D., D.I., N.G.); Department of Molecular Biology, Max Planck Institute for Developmental Biology, 72076 Tübingen, Germany (E.C., D.W.); and RIKEN Center for Sustainable Resource Science, Tsurumi, Yokohama, Kanagawa 230-0045, Japan (M.K., H.S.)

ORCID IDs: 0000-0003-4018-3705 (Y.J.N.); 0000-0003-2941-0233 (J.B.); 0000-0002-0889-9837 (E.C.); 0000-0001-6565-5145 (F.C.); 0000-0003-4762-6580 (V.S.); 0000-0003-4402-2191 (S.D.); 0000-0002-2114-7963 (D.W.); 0000-0002-3217-8407 (D.I.); 0000-0002-3946-1758 (N.G.).

Although phytohormones such as gibberellins are essential for many conserved aspects of plant physiology and development, plants vary greatly in their responses to these regulatory compounds. Here, we use genetic perturbation of endogenous gibberellin levels to probe the extent of intraspecific variation in gibberellin responses in natural accessions of Arabidopsis (*Arabidopsis thaliana*). We find that these accessions vary greatly in their ability to buffer the effects of overexpression of *GA20ox1*, encoding a rate-limiting enzyme for gibberellin biosynthesis, with substantial differences in bioactive gibberellin concentrations as well as transcriptomes and growth trajectories. These findings demonstrate a surprising level of flexibility in the wiring of regulatory networks underlying hormone metabolism and signaling.

The relationship between a phenotype and a specific genetic change, also referred to as expressivity, depends not only on the environment, but also on the genetic background in which a mutation occurs (Dowell et al., 2010; Chandler et al., 2013; Chari and Dworkin, 2013). Although typically treated as a nuisance by laboratory geneticists, such epistatic interactions are not only central to studies of genetic variation in populations, but can also increase our understanding of genetic networks and phenotypic robustness (Félix, 2007; Félix and Wagner, 2008; Paaby et al., 2015; Vu et al., 2015). Similar to its implications for human health (Schilsky, 2010), the accurate prediction of background-dependent phenotypic effects of specific mutations is of great interest to crop breeders.

Gibberellins (GAs) are phytohormones with well documented roles in germination, stem elongation, flowering, and leaf, seed, and fruit development, often in response to environmental changes (Hedden, 2003; Ueguchi-Tanaka et al., 2007; Schwechheimer and Willige, 2009; Claeys et al., 2014). In addition, roles in plant immunity have been discovered (De Bruyne et al., 2014). GA20-oxidase (GA20ox), a rate-limiting enzyme in the GA biosynthesis pathway, catalyzes consecutive oxidation events in the late steps of the formation of active GAs. It uses various intermediates as substrates, including GA_{12}, GA_{53}, GA_{15}, GA_{44}, GA_{24}, and GA_{19}, to finally form GA_9 and/or GA_{20} that are converted into bioactive GAs (Hedden and Thomas, 2012) by GA3-oxidase (GA3ox). In Arabidopsis (*Arabidopsis thaliana*), five genes encode GA20ox enzymes. In the Col-0 background, *GA20ox1*, *2*, and *3* are the dominant forms with an important role in growth and fertility, while *GA20ox4* and *5* have minor roles (Plackett et al., 2012). The mutation of *GA20ox1*, *2*, and *3* causes severe dwarfism and sterility (Rieu et al., 2008; Plackett et al., 2012), and overexpression of *GA20ox1* has been shown to enhance plant growth as a result of increased GA levels (Huang et al., 1998; Coles et al., 1999; Gonzalez et al., 2010; Nelissen et al., 2012).

Here, to assess natural variation in the ability to respond to changes in GA metabolism, we examined at

[1] This research received funding from the Bijzonder Onderzoeksfonds Methusalem Project (BOF08/01M00408). Work at the Max Planck Institute is supported by ERC Advanced Grant IMMUNEMESIS and the Max Planck Society.

[2] These authors contributed equally to the article.

[3] These senior authors contributed equally to the article.

[4] Present address: INRA Bordeaux-Aquitaine, 33140 Villenave d'Ornon, France.

* Address correspondence to dirk.inze@psb.vib-ugent.be.

The author responsible for distribution of materials integral to the findings presented in this article in accordance with the policy described in the Instructions for Authors (www.plantphysiol.org) is: Dirk Inzé (dirk.inze@psb.vib-ugent.be).

Y.-J.N. and D.H. were the main authors of this work; Y.J.N., E.C., M.K., S.D., J.B., and T.V.D. conducted experimental work; D.H., F.C., V.S., and Y.J.N. analyzed the data; D.H. and E.C. participated in discussions; D.I., N.G., D.W., and H.S. supervised the research; D.I., D.W., and N.G. contributed to writing the manuscript.

[OPEN] Articles can be viewed without a subscription.

www.plantphysiol.org/cgi/doi/10.1104/pp.16.01626

multiple levels the effect of the ectopic expression of *GA20ox1* in 17 Arabidopsis accessions. We found that in terms of leaf growth, the accessions respond differently to the increased expression of *GA20ox1*, although increased levels of the bioactive GA were quantified in all accessions. Our results indicate that hormone metabolism and signaling are remarkably different in these accessions.

RESULTS

Natural Variation in Growth and Hormone Content

Seventeen accessions from throughout the native range of the species (Supplemental Table S1) were grown for 25 d after stratification (DAS) in soil. Thirteen leaf size-related parameters were measured at rosette (fresh and dry weight, number of leaves, and total rosette area), leaf (first leaf pair area, vascular complexity, and density), and cellular level (stomatal index and density, epidermal pavement cell number, area, and circularity, and endoreduplication index of the first leaf pair). The 17 accessions, including the reference accession Col-0, varied for all parameters (Fig. 1A; Supplemental Table S2), differing more than 2.5-fold in rosette biomass, total rosette area, pavement cell number and area, stomatal density, and vascular complexity. Fresh weight showed a significant positive correlation with dry weight, total rosette area, leaf number, and leaf area and correlated negatively with vascular density and complexity (Supplemental Fig. S1).

To examine the potential link existing between growth variation in these accessions and phytohormone accumulation, we measured the levels of biosynthetic intermediates and different bioactive forms of GA, cytokinin, salicylic acid (SA), jasmonic acid (JA), abscisic acid (ABA), and auxin at 12 DAS (Fig. 1, B and C; Supplemental Table S3). GAs, SA, and the auxin indole-3-acetic acid (IAA) varied the most, while cytokinins and ABA varied the least, with JA showing an intermediate degree of changes (Fig. 1, B and C). In addition, we found that the relationships between different GAs and their intermediates, most of which are substrates of GA20ox, were complex. For example, the bioactive GA_4 showed a similar profile as its direct precursor, GA_9, but the levels of all other intermediates did not parallel that of GA_9 and GA_4 (Fig. 1B). Similarly, the bioinactive form GA_8 and its precursor GA_{19} showed a similar pattern of accumulation, while their intermediate forms, GA20 and GA1, were not detected (Fig. 1B). These observations suggest a different degree of GA20ox activity for GA biosynthesis in the different accessions. We analyzed the relationship between all the hormones measured using Pearson correlation, and only positive correlations were found between the different plant hormones (Supplemental Table S3; Supplemental Fig. S2).

We uncovered that three hormones, GA, iP, and IAA, were significantly positively correlated with pavement cell number, a leaf growth parameter (Supplemental Fig. S3). Furthermore, one of the GA20ox products, GA_{19}, and the GA bioinactive form, GA_8, were negatively correlated with the other two leaf growth parameters, endoreduplication index and stomatal index (Supplemental Fig. S3).

Consequences of *GA20ox1* Overexpression in Different Accessions

Overexpression of *GA20ox1* in the reference Col-0 background causes similar phenotypes as treatment with exogenous GA, such as larger rosette leaves, longer hypocotyls, increased height, and early flowering (Huang et al., 1998; Coles et al., 1999; Gonzalez et al., 2010; Nelissen et al., 2012; Ribeiro et al., 2012). To investigate natural genetic variation in phenotypic responses to GA level perturbance in Arabidopsis, we introduced the same overexpression construct into 16 additional accessions. In these accessions, the cDNA sequence of the *GA20ox1* showed only few differences that led to synonymous substitutions at protein level (Supplemental Fig. S4; Supplemental Table S4). Two to five independent homozygous lines for each accession were selected and grown in soil for 25 d.

Leaf and Rosette Area

Most, but not all, accessions visibly responded to *GA20ox1* overexpression, with altered rosette sizes and longer petioles (Fig. 2A). Importantly, the response was not always in the same direction. For example, whereas in the majority of accessions, the area of younger leaves was increased, in five accessions (An-1, L*er*-0, Blh-1, C24, and WalhaesB4) these leaves were smaller as compared with the corresponding wild-type controls (Fig. 2B; Supplemental Fig. S5; Supplemental Tables S5 and S6). Overall, for 10 accessions, transgenics had larger rosettes (Fig. 2C), as measured by rosette expressivity corresponding to the ratio of a transgenic line rosette area to that of the wild type. The penetrance, corresponding to the proportion of accessions showing an increased rosette area, was therefore 60%.

To test if the accessions show the same variation in response after exogenous treatment of GA, wild-type plants were grown in soil for 14 d and sprayed every 2 d with GA_3, and at 25 d, individual leaf area was measured. As shown in Supplemental Figure S6 (Supplemental Table S7), we observed that accessions for which a large decrease in leaf area was found upon *GA20ox1* overexpression (An-1, L*er*-0, Blh1, and C24) also showed a decrease in leaf area upon GA_3 treatment. Similarly, accessions for which transgenics showed the largest increase in leaf area (ICE61, ICE138, ICE97, or Oy-0) also presented an increase in leaf area when sprayed with GA_3. For few accessions (WalhaesB4 or Col-0), the effect was different between the transgenics and the GA-treated plants. This discrepancy might be explained by the fact that the treatment started at 14 d, while *GA20ox1* is overexpressed from the germination on.

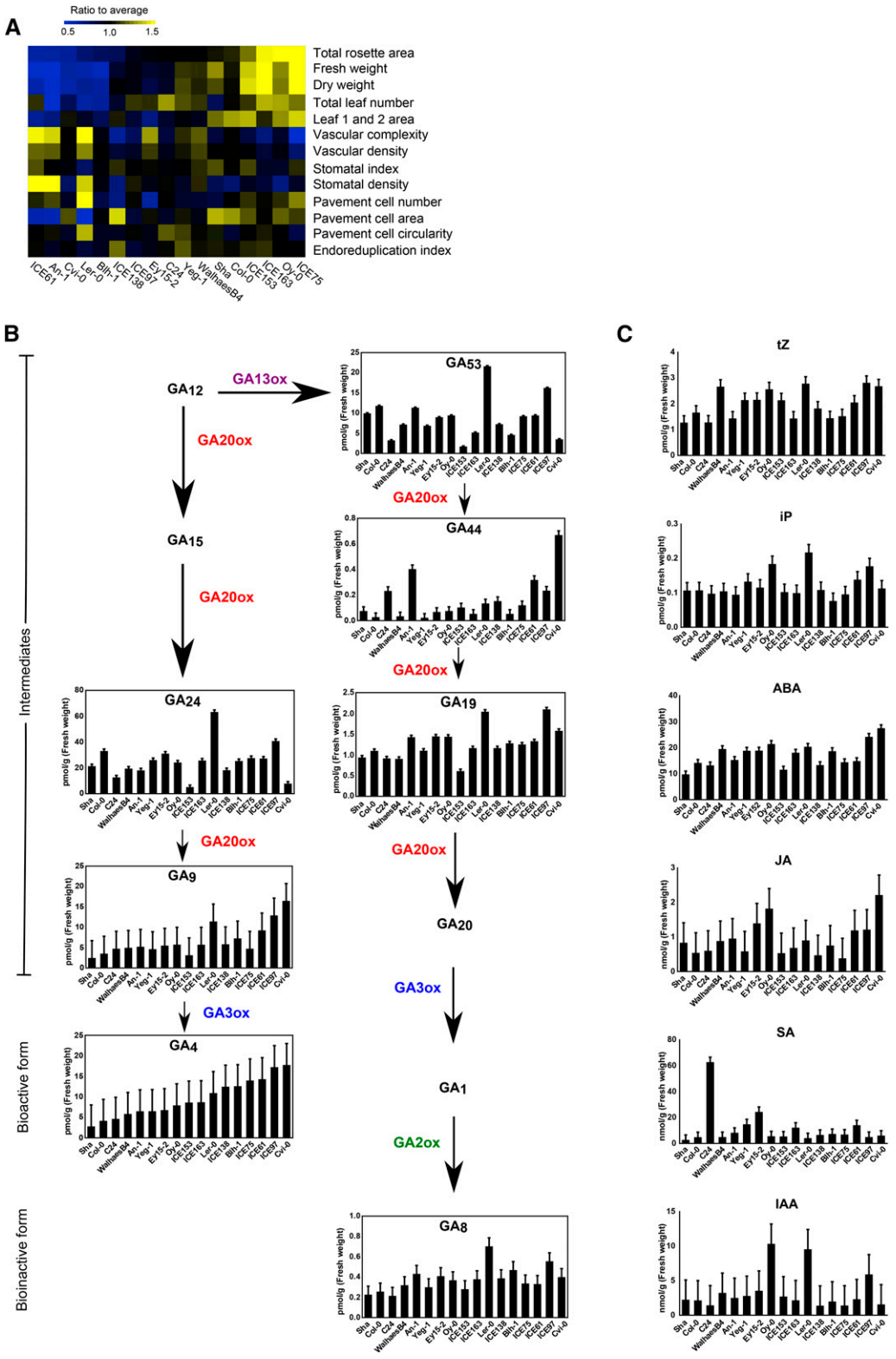

Figure 1. Variability in leaf size-related parameters and hormone content in 17 Arabidopsis accessions. A, Heat map representing the distance to the average of 17 accessions for 13 leaf size-related parameters ($n = 3$). Accessions are arranged based on the value of the rosette area. The measurements and calculations can be found in Supplemental Table S2. B, Basal GA levels in 17 accessions. GA biosynthesis (GA20ox and GA3ox) and catabolic (GA2ox) enzymes are indicated with different colors. GA20 and GA1 were not detected. C, Basal levels of cytokinins (tZ and iP), ABA, JA, SA, and IAA in the 17 accessions ($n = 3$). Error bars represent SE.

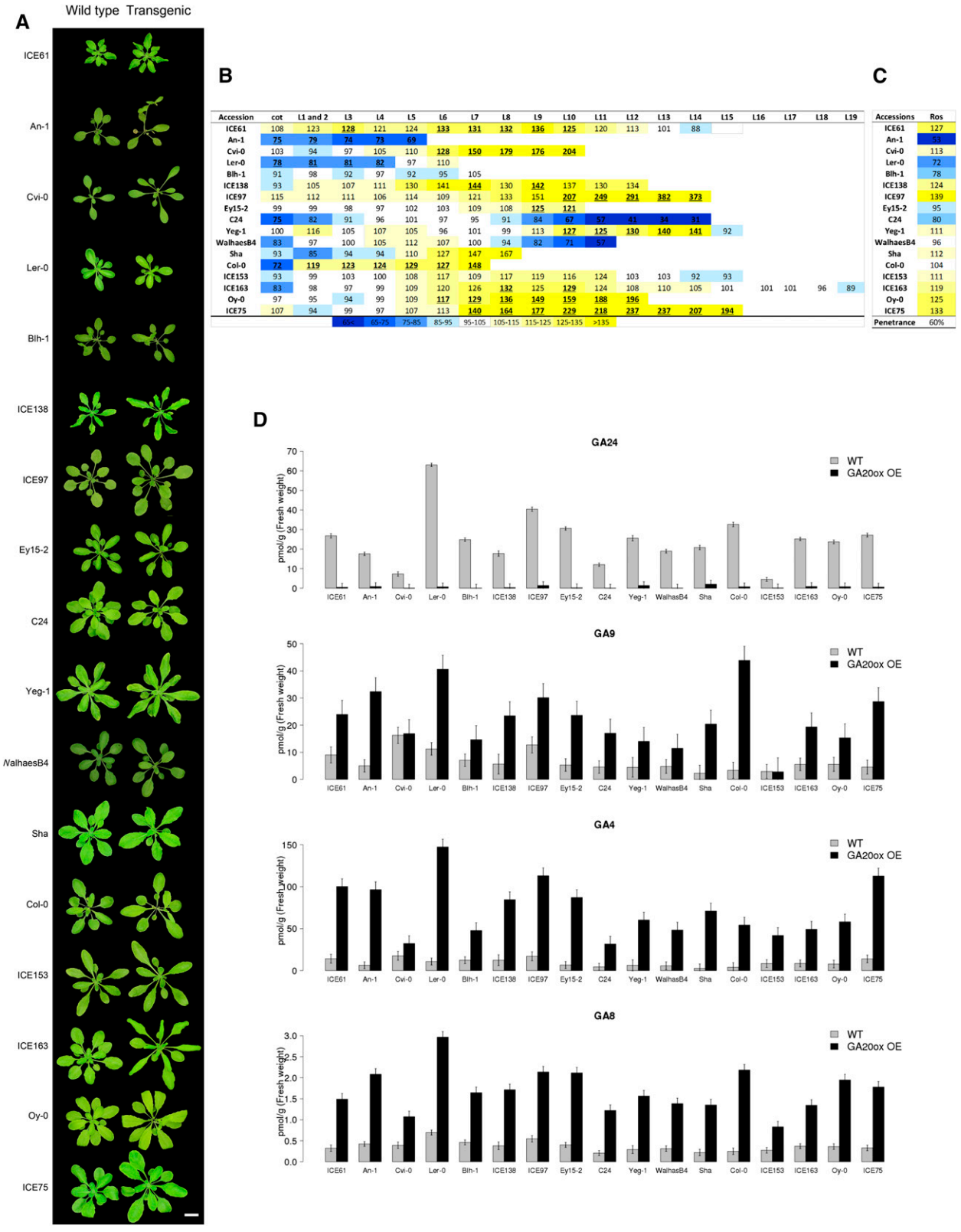

Accession	cot	L1 and 2	L3	L4	L5	L6	L7	L8	L9	L10	L11	L12	L13	L14	L15	L16	L17	L18	L19
ICE61	108	123	**128**	121	124	**133**	**131**	**132**	**136**	**125**	120	113	101	88					
An-1	**75**	**79**	**74**	**73**	**69**														
Cvi-0	103	94	97	105	110	**128**	**150**	**179**	**176**	**204**									
Ler-0	**78**	**81**	**81**	**82**	97	110													
Blh-1	91	98	92	97	92	95	105												
ICE138	93	105	107	111	130	141	**144**	130	**142**	137	130	134							
ICE97	115	112	111	106	114	109	121	133	151	**207**	**249**	**291**	**382**	**373**					
Ey15-2	99	99	98	97	102	103	109	108	**125**	**121**									
C24	**75**	82	91	96	101	97	95	91	84	**67**	**57**	**41**	**34**	**31**					
Yeg-1	100	116	105	107	105	96	101	99	113	**127**	**125**	**130**	**140**	**141**	92				
WalhaesB4	83	97	100	105	112	107	100	94	82	71	**57**								
Sha	93	**85**	94	94	110	127	147	167											
Col-0	**72**	**119**	**123**	**124**	**129**	**127**	**148**												
ICE153	93	99	103	100	108	117	109	117	119	116	124	103	103	92	93				
ICE163	83	98	97	99	109	120	126	**132**	125	**129**	124	108	110	105	101	101	101	96	89
Oy-0	97	95	94	99	109	**117**	**129**	**136**	**149**	**159**	**188**	**196**							
ICE75	107	94	99	97	107	113	**140**	**164**	**177**	**229**	**218**	**237**	**237**	**207**	**194**				
			65-	65-75	75-85	85-95	95-105	105-115	115-125	125-135	>135								

Accessions	Ros
ICE61	127
An-1	93
Cvi-0	113
Ler-0	72
Blh-1	78
ICE138	124
ICE97	139
Ey15-2	95
C24	80
Yeg-1	111
WalhaesB4	96
Sha	112
Col-0	104
ICE153	111
ICE163	119
Oy-0	125
ICE75	133
Penetrance	60%

Figure 2. Phenotype of *GA20ox1* overexpressing (OE) lines of 17 Arabidopsis accessions. A, Image of 25-d-old rosettes of representative *GA20ox1* OE lines and their corresponding wild type. Bar = 2 cm. B, Heat map representing, per accession, the average predicted percent difference in each leaf area between *GA20ox1* OE lines and their corresponding wild type. Bold with underline: P value < 0.05. C, Heat map showing the estimated expressivity and

In conclusion, we confirm that these accessions respond differently to changes in GA and that in the majority of the accessions the size of the young leaves is increased.

GA Levels

Next, we measured GA levels in the transgenic lines (Fig. 2E; Supplemental Fig. S7). We found that accumulation of GA20ox substrates GA_{53}, GA_{44}, GA_{19}, and GA_{24} was reduced, whereas GA20ox products GA_9 and GA_{20}, two bioactive forms, as well as GA_8, a bioinactive form of GA, were strongly increased in all transgenic accessions compared with their wild-type control. We noticed that, within each accession, the levels of GA_1, and also of GA_4, in the different transgenic lines were relatively constant. For example, similar high amounts of GA_4 were found in the five transgenics from L*er*-0, and this accumulation was 3-fold higher than the levels in the five transgenics from Blh-1. This constant level of accumulation suggests that the levels of these GAs are particularly well buffered within a given accession against different levels of *GA20ox1* overexpression. However, there was no correlation between GA levels and expressivity of the growth-related phenotype (Supplemental Table S8), indicating that the downstream growth responses differ across accessions.

We also found that rosette expressivity was significantly positively correlated with leaf number and fresh and dry weight of the wild-type accessions and negatively correlated with both vascular complexity and density (Supplemental Fig. S8).

In conclusion, *GA20ox1* overexpression causes distinct effects in different accessions, with the majority of accessions showing an enhanced leaf and rosette size.

Transcriptome Changes in Response to *GA20ox1* Overexpression

We used RNA-seq of 10 accessions and their representative transgenic derivatives with variable changes in leaf 6 area to profile differential downstream responses of *GA20ox1* overexpression. Because cell proliferation and/or cell expansion were affected in the transgenic lines (Fig. 2D) and the transition between cell proliferation and cell expansion is crucial for determining the final leaf size (Andriankaja et al., 2012; Gonzalez et al., 2012; Hepworth and Lenhard, 2014), leaves were microdissected (size <0.25 mm^2) at the beginning of this transition, either at 12 or 13 DAS depending on the accession (see Methods), and used for RNA-seq. At this time point, only *GA20ox1* and *2* were found to be expressed in the wild-type accessions with variable expression levels mainly for *GA20ox2* between the accessions (Supplemental Fig. S9). Because these two genes are the major expressed forms of the *GA20ox* gene family in the accessions used for RNA-seq, we also verified the sequence of *GA20ox2*. As for *GA20ox1*, we found small changes between the accessions in the cDNA sequences that led to synonymous changes (Supplemental Fig. S10).

RNA-seq first confirmed overexpression of *GA20ox1* in all transgenic lines (Supplemental Fig. S11), but this was not predictive of bioactive GA_4 levels as measured by a nonsignificant Pearson correlation of 0.211. Consistent with the morphological observations, accession-specific properties dominated over the effects of *GA20ox1* overexpression, as deduced from the principal component analysis (PCA; Fig. 3A; Supplemental Fig. S12).

To identify differentially expressed genes, we considered transgenic lines of a particular accession as repeats of a single line because one sample per genotype was sequenced. Because only one wild-type sample per accession was sequenced, the experimental setup did not allow the identification of an accession-specific response. We therefore performed a statistical test to identify a general differential response between wild types and transgenic lines over the 10 accessions. A total of 730 genes were identified as differentially expressed (DE) with 361 with a fold change higher or lower than 1.5. Overrepresented Gene Ontology (GO) categories were photosynthesis, secondary metabolism, protein and hormone metabolism, regulation of transcription, transport, amino acid metabolism, and sulfur assimilation pathways (Fig. 3, B and C; Supplemental Table S9; Supplemental Fig. S13). Genes involved in GA deactivation and degradation (*GIBBERELLIC ACID METHYLTRANSFERASE2*, *GA2ox1*, and *GA2ox4*) were up-regulated, and GA biosynthetic genes *GA3ox1* and *GA20ox2* were down-regulated in many lines, indicative of feedback regulation (Fig. 3B). Several genes related to other phytohormones, including JA, ABA, brassinosteroid, auxin, ethylene, and cytokinin, were altered in expression, reflecting extensive cross-regulation among hormones (Weiss and Ori, 2007). For example, six small auxin up-regulated RNAs (*SAUR*), two ethylene response factors (*ERF*), and 9-cis-epoxycarotenoid dioxygenase (*NCED*), a gene encoding a rate-limiting enzyme in ABA biosynthesis, were differentially expressed in the *GA20ox1* overexpression lines. Genes related to photosynthesis were mostly down-regulated (Fig. 3C). Because we analyzed young developing leaves, a possible explanation is that GA promotes growth and delays the onset of differentiation and the establishment of the photosynthetic apparatus by decreasing leaf chlorophyll content (Cheminant et al., 2011).

Figure 2. (*Continued.*)
penetrance (Sel, selective; Ros, rosette; see "Materials and Methods") of *GA20ox1* OE. D, GA levels in *GA20ox1* OE lines. The normalized values represent the average concentrations between all transgenics for one accession and are represented with SE bars ($n = 3$).

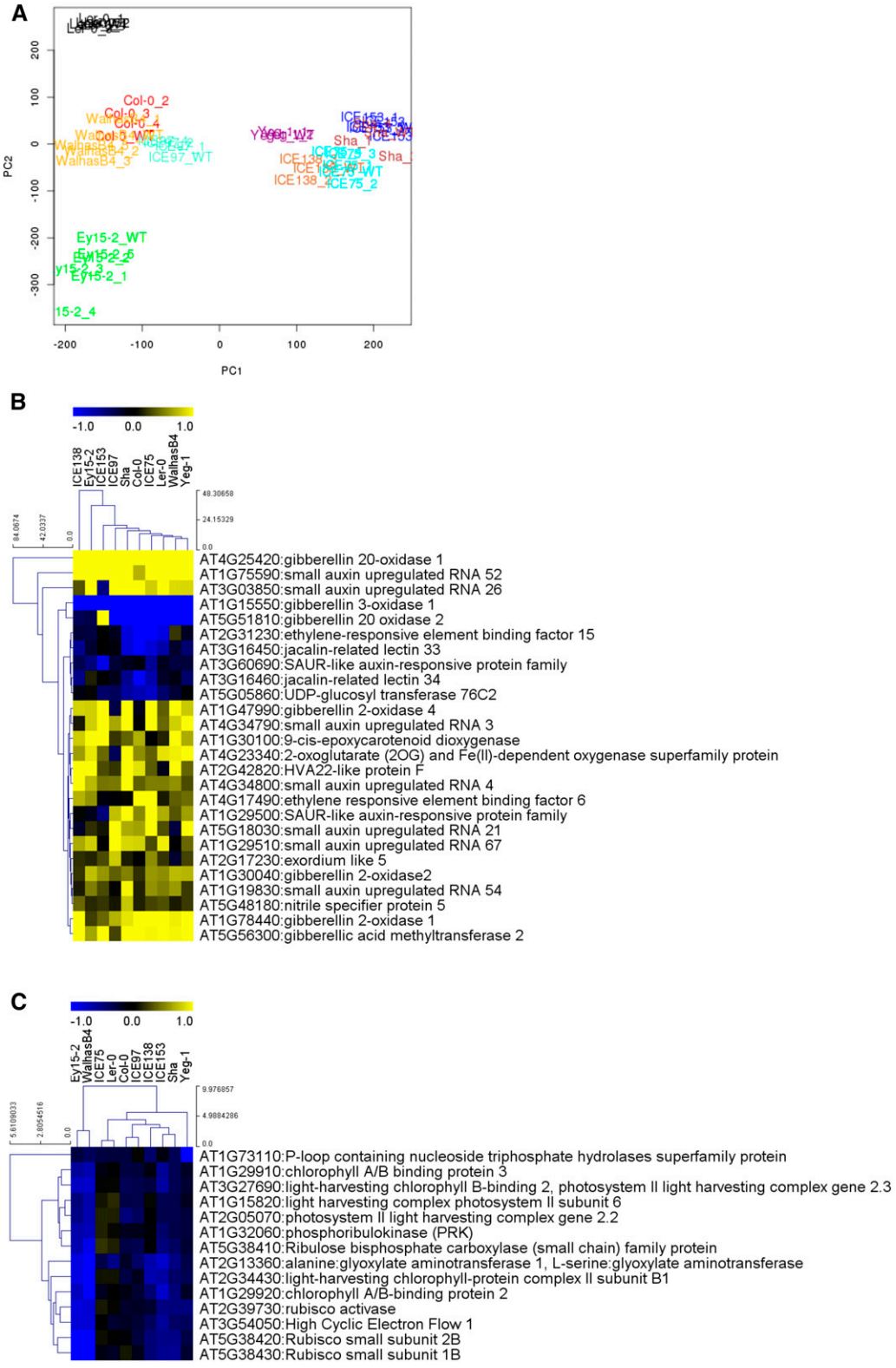

Figure 3. PCA of transcriptomics data and heat maps representing the fold change of differentially expressed genes in *GA20ox1* OE lines. A, PCA plot representing classifications of transcriptomics data of wild-type and *GA20ox1* OE lines. Each accession is displayed in a different color. W, wild type; 1-5, independent transgenic lines. B and C, Differentially expressed genes involved in hormone metabolism (B) and photosynthesis (C). Yellow and blue colors represent increased and decreased expression, respectively, in comparison with the wild types. Only DE genes that show at least 1.5-fold change difference are shown. Hierarchical clustering was done for both genes and samples with Manhattan distance metrics.

To identify genes for which the expression pattern could be linked to the degree of response to the transgenes, we estimated correlation between changes in expression and rosette expressivity. This correlation analysis identified 132 genes that were either significantly positively (71) or negatively (61) correlated with expressivity of morphological effects (Fig. 4). The genes with an expression positively correlating with rosette expressivity belonged to various GO categories, such as regulation of programmed cell death or regulation of response to drug or glycerol catabolic process, while the function of genes negatively correlated was related to circadian rhythm, response to organic stimulus, response to stress, and response to hormone, auxin, ethylene, and salicylic acid but also gibberellin (Supplemental Fig. S14). Among these genes, 13 were found to be significantly differentially expressed with a fold change higher or lower than 1.5.

We speculate that these genes (discussed below) might have important roles in determining the influence of *GA20ox1* overexpression in the different accessions.

DISCUSSION

Overexpression of *GA20ox1* in 17 accessions increased the levels of the bioactive forms of GA (GA_1 and GA_4) and depleted GA_{24}, the direct precursor of GA_4, in all accessions, demonstrating that the *GA20ox1* transgene is active in all accessions. A remarkable observation was that the levels of GA_1 and GA_4 are very similar across multiple transgenic lines of an accession. In other words, there appears to be an accession-specific maximum accumulation level of GA_1 and GA_4. The reason for this is currently unclear, but it is known that bioactive GA forms stimulate the expression and activity of GA catabolism, counteracting the accumulation of the bioactive GAs and converting GA to bioinactive forms such GA8. Furthermore, GA represses the expression of endogenous genes encoding the GA biosynthetic genes *GA20ox* and *GA3ox* (Coles et al., 1999; Nelissen et al., 2012; Ribeiro et al., 2012). Such feedback regulation was also observed in the transcriptomics data of the *GA20ox1* overexpression lines in all accessions analyzed. Possibly, there is an accession-specific feedback control in which the GA receptors and the GA-triggered degradation of DELLA proteins likely play a role (Ueguchi-Tanaka et al., 2007; Claeys et al., 2014). Although the majority of accessions showed a positive effect on leaf growth upon introduction of the *GA20ox1* transgene, the effect quantitatively differed between accessions, and in some accessions, *GA20ox1* overexpression had even a negative effect on leaf and rosette size. We confirmed this effect when wild-type plants were treated with GA_3. However, no clear correlation could be found between the levels of *GA20ox1* overexpression or the levels of various GAs and the observed effects. Similar genotype-dependent effects on freezing tolerance have been found when the cold tolerance genes *CBF1*, *CBF2*, and *CBF3* were down-regulated in eight different accessions of Arabidopsis (Gery et al., 2011).

We also observed that the biomass of the wild-type accessions was positively correlated with the growth-promoting effect of *GA20ox1* overexpression on rosette size. Accessions with larger rosettes showed a more pronounced response to *GA20ox1* overexpression than those with smaller rosettes. We hypothesize that in large accessions, the growth-regulatory network is less constrained and more prone to the effect of positive growth regulators, whereas in small accessions, which have a more restrictive growth network, it would be more difficult to make larger plants. In addition, it seems that there is more room for physical expansion in larger accessions because vascular density and complexity in the wild-type accessions showed a negative correlation with rosette expressivity. For rosette expressivity, no direct correlation with GA levels was found. A possible reason for this observation is that rosette size is a complex trait determined by many different factors, among which leaf number and size and speed of development that therefore has to integrate different individual organs.

How can we explain the natural variation in the effect of *GA20ox1* overexpression based on our finding of almost no strong correlation between its transcript level, active GA quantities, and phenotypic effects? Because many steps exist between the expression of *GA20ox1* and its actual effect on growth, differences in signal transduction along the GA pathway, depending on the genetic background, could therefore be the reason for the observed variability. First, translatome analysis after treatment with bioactive GAs has revealed that differential mRNA translation, possibly varying between the different accessions, is important for the control of feedback regulation of GA-related genes (Ribeiro et al., 2012). Second, at the protein level, the amount of the GA-receptor (GID) and DELLAs, which are negative regulators of GA signaling, their affinity, and their efficiency to form the regulatory module GA-GID-DELLA might be different in the different accessions and, therefore, differentially affect the response. Distinct interactions with other growth regulatory elements could also explain the variation observed. It has been shown, in Col-0, that overexpression of *GA20ox1* in binary combination with an altered expression of growth-promoting genes leads to different size phenotypes in function of the gene combination (Vanhaeren et al., 2014). It is therefore possible that differences in expression of growth regulatory genes, triggering different cellular characteristics in the wild-type plants, differently influence the effect of *GA20ox1* overexpression. In addition, we identified 132 genes of which the expression levels are correlated with the phenotypic expressivity of *GA20ox1* in all analyzed accessions. Interestingly, among the genes having an expression pattern negatively correlated with the degree of response to *GA20ox1*, several are related to the response to hormone stimulus and especially to GA. For example, *XERICO* (AT2G04240), known to be up-regulated by DELLA and repressed by GA and to

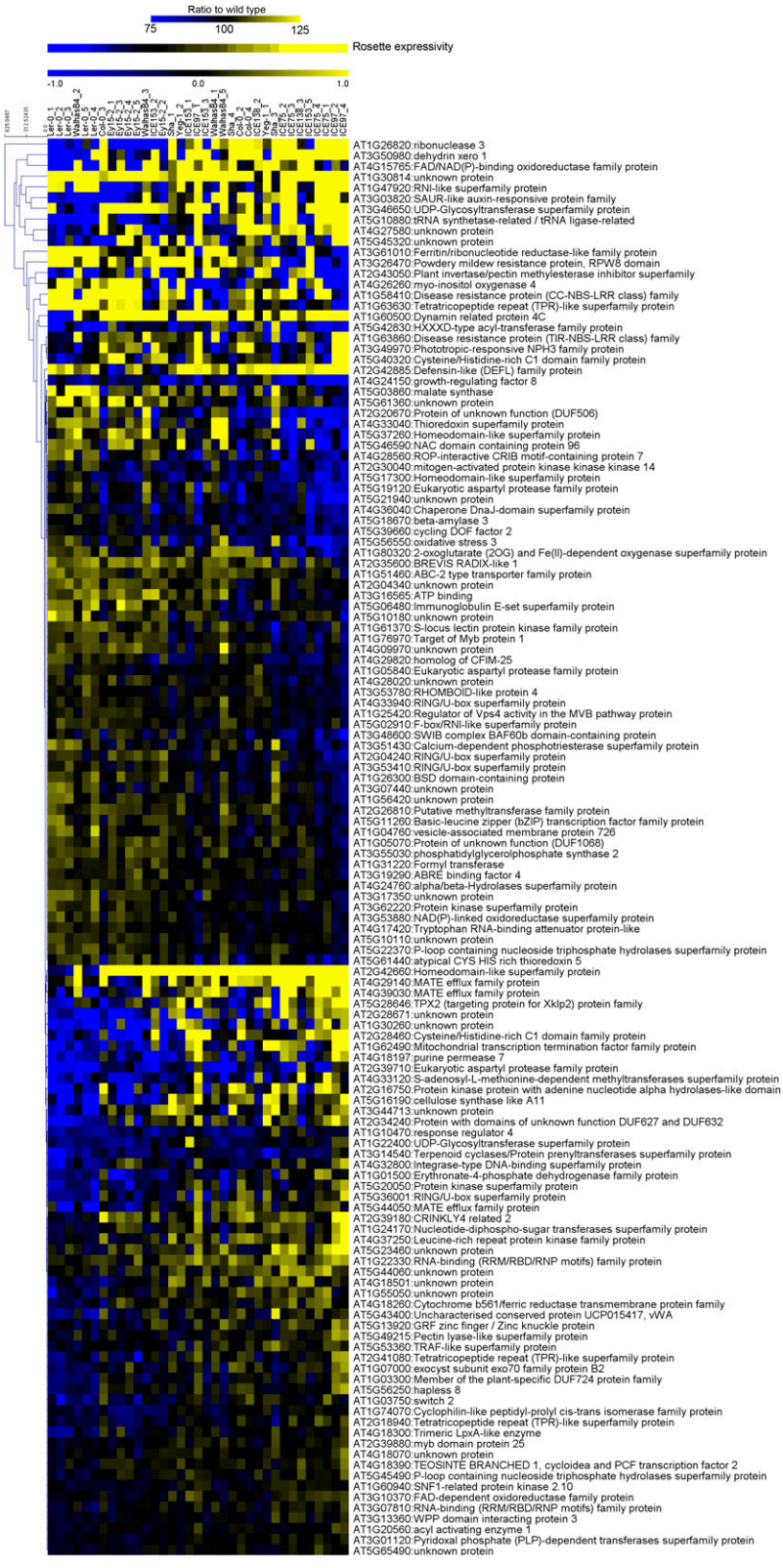

Figure 4. Correlation analysis between phenotypic and transcriptomic data. Heat maps represent the DE genes correlated with rosette expressivity and the expressivity of the rosette leaves. Yellow and blue correspond to increased and decreased expression, respectively, in comparison with the wild type. The DE genes with at least 1.5-fold change are indicated with an asterisk. Hierarchical clustering was done for genes with Manhattan distance metrics. Samples were ordered in function of the expressivity (correlation coefficient $> |0.5|$, adj-P value < 0.05).

promote accumulation of ABA (Zentella et al., 2007), is more or less expressed in the accessions presenting the smallest or largest rosette expressivity, respectively. In addition, few of the correlated genes have previously been associated with plant growth. For example, *GRF8* (*AT4G24150*) is one of the nine members of the *GROWTH*

REGULATING FACTOR gene family with a major role in regulating cell proliferation and/or cell expansion during plant development (Kim et al., 2003; Vercruyssen et al., 2014). Two auxin-related genes were also found to correlate with rosette expressivity: *ARABIDOPSIS ABNORMAL SHOOT3* (*AT4G29140*; Li et al., 2014) and *REVEILLE1* (*AT5G17300*; Rawat et al., 2009). Interestingly, it has been shown that *REVEILLE1* binds to the promoter of GIBBERELLIN 3-OXIDASE2, can inhibit its transcription, and therefore suppresses the biosynthesis of GA (Jiang et al., 2016). Further work is required to determine whether this subset of genes has, either alone or in combination, a functional role in determining the accession-specific responses to elevated GA levels.

CONCLUSION

Plant growth is regulated by complex molecular networks that are determined by the genome and its interaction with the ever-changing environment. Such growth regulatory networks are expected to be rather different among species and even within a species, which might serve as a key element in adaptation to different environments. It has been demonstrated that mutations or transgenes influencing growth might have different effects in different genetic backgrounds in several model organisms (Dowell et al., 2010; Chandler et al., 2013). Here, we show for 17 different Arabidopsis accessions that the ectopic expression of a rate-limiting enzyme for gibberellin biosynthesis has very different effects on growth depending on the accession in which the gene is introduced. Most accessions visibly responded by changing their growth especially with an altered leaf size and shape. However, across the accessions, the response did not always correspond to a positive effect on growth. Ten accessions showed larger rosettes whereas others had smaller rosette size compared to the wild type. We observed that in all transgenic lines, GA levels showed the same direction of accumulation, suggesting that GA biosynthesis/metabolism pathway is commonly changed across the accessions. Remarkably, transcript levels of *GA20ox1* did not correlate with the levels of bioactive GA. Furthermore, the levels of bioactive GA forms in the different transgenic lines were remarkably constant for all transgenics in each accession, suggesting the existence of an accession-specific plateau for maximal accumulation of these GAs. GA levels were therefore not correlated with the phenotypes, suggesting that a high accumulation level of GA is not always responsible for a positive growth regulation.

In order to provide further insight into the mechanism that is behind the accession-specific effect of GA perturbation, screening for modifier genes that suppress the response to GA perturbation in transgenic lines of a specific accession could be performed. Furthermore, detailed analysis of the GA signaling pathway in the different accessions is likely to shed light on how GA affects growth to a very different extent in different Arabidopsis accessions.

MATERIALS AND METHODS

Plant Material and Growth Conditions

Seventeen Arabidopsis (*Arabidopsis thaliana*) accessions were selected to cover most common genetic variants of Arabidopsis (Supplemental Table S1) and used to generate *GA20ox1*-overexpressing lines. cDNA of the full *GA20ox1* coding region from Col-0 was cloned in the fluorescence-accumulating seed technology vectors (Shimada et al., 2010) and introduced into the 17 accessions following the floral dip protocol (Clough and Bent, 1998). Dried transgenic T1 seeds were selected based on fluorescence signal in the seed coat and sown on soil for seed production. T2 transgenic seeds were harvested, and selection of five independent single-locus insertion lines (75% of fluorescent seeds) was done. Seeds were sown on soil for seed production, and expression of the transgene was verified by RT-qPCR. From these lines, at least two and maximum five independent T3 homozygote lines for each accession were selected for further experiments. All plants were grown in soil under a 16-h-day/8-h-night regime at 21°C in a growth chamber.

For GA treatments, the 17 accessions were grown in soil until 14 d after stratification, and plants were sprayed every second day with 1 mL of 50 μM GA_3 containing 0.1% (v/v) Tween 80 or mock (Ribeiro et al., 2012). Leaf series were made when plants were 25 d old.

Phenotypic Analysis

Measurement of 13 Leaf Size-Related Parameters in 17 Accessions

Twenty four plants for each accession were grown in soil for 25 d in three independent experiments. Plants were randomly distributed. Fresh and dry weight was measured from 8 to 12 plants, and leaf series were made by dissecting individual leaves from 8 to 12 plants and mounting them on a 1% agar plate. The area of each individual leaf was measured with the ImageJ software (http://rsb.info.nih.gov/ij/). Total rosette area and total leaf number were calculated from the leaf series analysis. Measurements of venation patterns were done as previously described (Dhondt et al., 2012) from leaves 1 and 2. The cellular analysis on leaves 1 and 2 was done as previously described (Andriankaja et al., 2012) and allowed calculating pavement cell number, area, and circularity and stomatal index and density. Ploidy levels of leaves 1 and 2 were measured, and the endoreduplication index was calculated as previously described (Claeys et al., 2012). The measurements of fresh and dry weight, total leaf number, leaves 1 and 2, total rosette area, and endoreduplication index were obtained from the three repeats. The cellular analysis and the vasculature analysis were done for two repeats from five leaves for each repeat. For the heat map of leaf size-related parameters (total rosette area, fresh weight and dry weight of the shoot, total number and area of leaves, pavement cell number and area, cell circularity, endoreduplication index, stomatal density, stomatal index, and vascular complexity and density of leaves 1 and 2) in the 17 accessions, the measured value for a parameter in each accession was divided by the average of this parameter for all accessions.

Measurement of Leaf Area in the Transgenic Lines

Ten plants per genotype were grown in a randomized manner for 25 d in soil. All the independent transgenics for an accession were grown in the same experiment together with their corresponding wild type. Separate experiments for each natural accession were conducted. Leaf series were made by dissecting individual leaves from 10 plants, and the leaf area was measured with the ImageJ software.

To evaluate the response to the transgene and therefore to estimate the effect of the transgene in the background of the natural accession versus the untransformed natural accession on each leaf, leaf area was log transformed to stabilize the variance. Data were truncated so that there were at least two observations for each leaf of both the transgenic lines and the corresponding wild type. The mean model consisted of the main effects of *GA20ox1* overexpression on leaf size and their interaction term. Due to the unbalanced and complex nature of the data, the Kenward-Rogers approximation for computing the denominator degrees of freedom for the tests of fixed effects was used. An autoregressive structure was used to model the correlations between measurements done on the leaves originating from the same plant. The main interest was in the effect of the gene on leaf area for each leaf separately. Simple tests of effects were performed at each leaf between the transgenic lines and the

corresponding wild type. Difference estimates were represented as percentage of the least-square means estimate of the wild type and leaf. The analysis was performed with the mixed and plm procedure of SAS (version 9.4 of the SAS System for Windows 7, 64 bit; SAS Institute).

Rosette expressivity is defined as the ratio of a transgenic line rosette area to that of the wild type. In the case of rosette expressivity per accession, the mean of rosette expressivity per transgenic line for an accession has been taken.

Hormone Analysis

The shoot of seedlings grown in soil until stage 1.03 (Boyes et al., 2001; 12 DAS for Cvi-0 and 11 DAS for the other accessions) was harvested in the middle of the day for three independent experiments and frozen in liquid nitrogen. The phytohormones GA (GA_4, GA_8, GA_9, GA_{19}, GA_{24}, GA_{44}, and GA_{53}), IAA (IAA, IAAsp, IAIle + IALeu, and IAPhe), ABA, SA, cytokinin (tZ, tZR, tZRPs, cZ, cZR, cZRPs, DZ, DZR, DZRPs, iP, iPR, iPRPs, tZ7G, tZ9G, tZOG, tZROG, cZROG, tZRPsOG, DZ9G, iP7G, and iP9G), and JA were measured as described previously (Kojima et al., 2009; Shinozaki et al., 2015). The hormone data were modeled with a linear model with accession as main factor and experiment as fixed block factor due to small number of samples (three repeats). The model was fitted with the lm function from the R software (v 3.0.1; R Core Team, 2015). Least squares means and standard errors were calculated with the lsmeans function of the lsmeans library (v. 2.10; Lenth and Hervé, 2014) from the R software (v 3.0.1; R Core Team, 2015). These estimates were used in Pearson correlation analyses.

RNA Extraction

Total RNA was extracted from the shoot of 12-d-old seedlings of T2 transgenic lines and the corresponding wild-type plants according to a combined protocol of TRIzol (Invitrogen) and the RNeasy kit (Qiagen) with on-column DNase (Qiagen) digestion. The expression of the transgene was analyzed by RT-qPCR. RT-qPCR was performed as previously described (Claeys et al., 2012).

For RNA-seq analysis, seedlings with one biological repeat of wild-type plants and *GA20ox1*-overexpressing lines (at 12 DAS for Col-0 and Ey15-2 and at 13 DAS for WalhaesB4, ICE97, ICE138, ICE75, L*er*-0, Yeg-1, Sha, and ICE153) were harvested in RNA ice-later solution (AM7030; Ambion) and incubated at −20°C for at least a week. Leaf 6 was microdissected on a cold plate with dry ice under a stereomicroscope and frozen in liquid nitrogen. RNA was extracted according to a combined protocol of TRIzol (Invitrogen) and the RNeasy kit (Qiagen) with on-column DNase (Qiagen) digestion. RNA was quantified and the quality was checked with a 2100 Bioanalyzer (Agilent).

RNA-Seq Analysis

Library preparation was done using the TruSeq RNA Sample Preparation Kit v2 (Illumina). In brief, poly(A)-containing mRNA molecules were reverse transcribed, double-stranded cDNA was generated, and adapters were ligated. After quality control using the 2100 Bioanalyzer, clusters were generated through amplification using the TruSeq PE Cluster Kit v3-cBot-HS kit (Illumina) followed by sequencing on a Illumina HiSeq 2000 with the TruSeq SBS Kit v3-HS (Illumina). Sequencing was performed in paired-end mode with a read length of 50 bp. The quality of the raw data was verified with FastQC (http://www.bioinformatics.babraham.ac.uk/projects/fastqc/; version 0.9.1). Next, quality filtering was performed using the FASTX toolkit (http://hannonlab.cshl.edu/fastx_toolkit/; version 0.0.13): Reads where globally filtered in which for at least 75% of the reads the quality exceeds Q20, and 3′ trimming was performed to remove bases with a quality below Q10. Repairing was performed using a custom Perl script. Reads were subsequently mapped to the Arabidopsis reference genome (TAIR10) using GSNAP (Wu and Nacu, 2010; version 2011-12-28) allowing maximally two mismatches. The concordantly paired reads that uniquely map to the genome were used for quantification on the gene level with htseq-count from the HTSeq.py python package (Anders et al., 2015). The analysis was implemented as a workflow in Galaxy (Goecks et al., 2010).

For the visualization of RNA-seq expression data and correlation analysis, count data were normalized following the normalization pipeline with the trimmed mean of M-values algorithm as implemented in the edgeR library from the R software (v.3.0.1; R Core Team, 2015). Weakly expressed genes were previously filtered out by removing genes that have less than five samples with an expression level lower than 0.5 counts per million. The 0 counts of normalized data were substituted with value 1-e10 and then the whole data set was $\log_2$ transformed.

The PCA plot on transformed count data were done in R software (v.3.0.1; R Core Team, 2015) using the "prcomp" function.

Differential Expression Analysis

Differential expression analyses of RNA-seq data were conducted with the EdgeR library (v.3.4.2) of the Bioconductor software from the R software (v.3.0.1; R Core Team, 2015). Filtering and normalization were performed as previously described. In this analysis, we consider transgenic lines of a particular accession as repeats of a single line; otherwise, we would not be able to run statistical tests because we have a single repeat per line. A statistical test for general, mean differential expression between wild types of accessions and transgenic lines of these accessions was performed using the glmLRT function with a contrast (Accession1_WT – Accession1_OE) + Accession2_WT – Accession1_OE) +…. + (AccessionN_WT – AccessionN_OE). For further analysis, genes were selected based on their false discovery rate adjusted *P* value lower than 0.05 and/or fold change threshold between transgenic lines and the wild type. The filter on the fold change requires a fold change higher than 1.5 for each transgenic line of an accession in at least one accession.

Enrichment analysis was done in MapMan (Ramšak et al., 2014; http://mapman.gabipd.org/) with significantly DE genes.

Heat maps are generated in Mev (v 4.9; Howe et al., 2011) for significantly DE genes filtered for and a 1.5-fold change threshold between transgenic lines and the wild type. Hierarchical clustering was done for both genes and samples with Manhattan distance metrics in Mev (v 4.9; Howe et al., 2011).

Sequence Extraction and Alignment

The sequences from AT4G25420 and AT5G51810 were extracted from the RNA-seq data. After preprocessing and mapping of the reads to the TAIR10 genome, sorting and deduplication of the read libraries were performed using picard v1.129 (http://broadinstitute.github.io/picard/). GATK v3.3.0 was used for variant calling (Van der Auwera et al., 2013). Analysis was based on recommendations in "Best Practices for RNA-seq" (https://www.broadinstitute.org/gatk/guide/best-practices?bpm=RNAseq). Before variant calling was performed, the different libraries were preprocessed using the tools splitnCigar, haplotypecaller, realignertargetcreator, indelrealigner, baserecalibrator, and printreads. In the haplotypecaller step, only high-quality scores were considered by setting a quality of 50. Next, a multisample variant calling was performed using haplotypecaller. In this step, all samples are analyzed together. Variants were filtered using VariantFiltration with the options -window 35, -cluster 3, -filterName FS, -filter "FS > 30.0", -filterName QD, and -filter "QD < 2.0." The resulting variants file was split by sample using bcftools (http://github.com/samtools/bcftools). Sequences were extracted for the genes (AT4G25420 and AT5G51810) using the alternative alleles for each sample using the GATK tool Fasta Alternate Reference Maker (Van der Auwera et al., 2013) and based on the Coding DNA Sequence coordinates (based on the structural annotation of TAIR10). The reverse complement was generated for genes located at the negative strand and subsequently protein sequences were extracted using custom scripts.

To align the extracted sequences, CLC main Workbench 6.0 was used (CLC bio, a Qiagen Company).

Correlation Analysis

Pearson correlation coefficient tests were run independently between phenotypes, between phenotypes and hormones, between hormones, and between penetrance and RNA-seq fold change data. Pearson correlation coefficients were calculated with corr.test function in R. The adjusted *P* values of correlations were calculated with a permutation test. We permuted a tested trait and ran correlation tests over the whole considered data set. Such a run was repeated 1000 times. The adjusted *P* values are calculated from all runs over all repeats as a proportion of correlation coefficients correlated in a higher degree than a tested correlation (r) to the number of permuted correlations (n), with a formula $(r + 1)/(n + 1)$ (North et al., 2002). The significant correlations, false discovery rate < 0.05, were visualized in Cytoscape (Cline et al., 2007).

Supplemental Data

The following supplemental materials are available.

Supplemental Figure S1. Correlation between the shoot-related phenotypic measurements of the 17 Arabidopsis accessions.

Supplemental Figure S2. Correlation between four of the major bioactive hormones (ABA, cytokinin, JA, and ABA) in 17 Arabidopsis accessions.

Supplemental Figure S3. Correlation between the leaf size-related parameters and hormones in the 17 Arabidopsis accessions.

Supplemental Figure S4. Sequence alignments of *GA20ox1* cDNA and the corresponding protein from 16 of the 17 Arabidopsis accessions studied.

Supplemental Figure S5. Heat map representing, per accession, the predicted percent difference in each leaf area between each independent *GA20ox1* OE lines and their corresponding wild type.

Supplemental Figure S6. Heat map representing, per accession, the percentage of difference in each leaf area between plants sprayed with GA_3 (GA) and the control plants (mock).

Supplemental Figure S7. GA levels in *GA20ox1* OE lines from the 17 Arabidopsis accessions.

Supplemental Figure S8. Correlation analysis of phenotypic data.

Supplemental Figure S9. *GA20ox1* and *GA20ox2* expression levels in the 10 Arabidopsis accessions used for RNA-seq.

Supplemental Figure S10. Sequence alignments of *GA20ox2* cDNA and the corresponding protein from 10 of the 17 Arabidopsis accessions studied.

Supplemental Figure S11. *GA20ox1* expression level in the transgenic lines from 10 Arabidopsis accessions.

Supplemental Figure S12. Variance explained by first 20 components for the RNA-seq analysis from the 10 accessions.

Supplemental Figure S13. Heat maps representing the fold change of DE genes in GA20ox1 OE lines.

Supplemental Figure S14. Overrepresented GO categories (biological process) for genes positively and negatively correlated with rosette expressivity.

Supplemental Table S1. Geographic origin of the 17 Arabidopsis accessions used in this study.

Supplemental Table S2. Measurements of 13 leaf size-related parameters in 17 accessions.

Supplemental Table S3. Correlation between levels of different hormones in the 17 Arabidopsis accessions.

Supplemental Table S4. Percentage differences between the sequences of GA20ox1 in 15 accessions and Col-0 at DNA and protein level.

Supplemental Table S5. Average individual leaf area (cot = cotyledon; L1 to L21 = leaf 1 to leaf 21) in the independent GA20ox1 overexpressing lines (E1 to E5) and their respective wild-type accessions.

Supplemental Table S6. Average values given as least square means predicted according to the statistical models and variation.

Supplemental Table S7. Average leaf area values given as least square means predicted according to the statistical models and variation.

Supplemental Table S8. Pearson correlation between the rosette expressivity after GA20ox1 overexpression and GA levels in the transgenics.

Supplemental Table S9. Overrepresented MapMan categories for *GA20ox1* DE genes.

ACKNOWLEDGMENTS

We thank the Systems Biology of Yield group for help with experiments and many discussions. We also thank Dr. Annick Bleys and Dr. Bram Slabbinck for help in improving the article.

Received October 20, 2016; accepted November 18, 2016; published November 22, 2016.

LITERATURE CITED

Anders S, Pyl PT, Huber W (2015) HTSeq–a Python framework to work with high-throughput sequencing data. Bioinformatics **31:** 166–169

Andriankaja M, Dhondt S, De Bodt S, Vanhaeren H, Coppens F, De Milde L, Mühlenbock P, Skirycz A, Gonzalez N, Beemster GTS, Inzé D (2012) Exit from proliferation during leaf development in *Arabidopsis thaliana*: a not-so-gradual process. Dev Cell **22:** 64–78

Boyes DC, Zayed AM, Ascenzi R, McCaskill AJ, Hoffman NE, Davis KR, Görlach J (2001) Growth stage-based phenotypic analysis of Arabidopsis: a model for high throughput functional genomics in plants. Plant Cell **13:** 1499–1510

Chandler CH, Chari S, Dworkin I (2013) Does your gene need a background check? How genetic background impacts the analysis of mutations, genes, and evolution. Trends Genet **29:** 358–366

Chari S, Dworkin I (2013) The conditional nature of genetic interactions: the consequences of wild-type backgrounds on mutational interactions in a genome-wide modifier screen. PLoS Genet **9:** e1003661

Cheminant S, Wild M, Bouvier F, Pelletier S, Renou J-P, Erhardt M, Hayes S, Terry MJ, Genschik P, Achard P (2011) DELLAs regulate chlorophyll and carotenoid biosynthesis to prevent photooxidative damage during seedling deetiolation in *Arabidopsis*. Plant Cell **23:** 1849–1860

Claeys H, De Bodt S, Inzé D (2014) Gibberellins and DELLAs: central nodes in growth regulatory networks. Trends Plant Sci **19:** 231–239

Claeys H, Skirycz A, Maleux K, Inzé D (2012) DELLA signaling mediates stress-induced cell differentiation in Arabidopsis leaves through modulation of anaphase-promoting complex/cyclosome activity. Plant Physiol **159:** 739–747

Cline MS, Smoot M, Cerami E, Kuchinsky A, Landys N, Workman C, Christmas R, Avila-Campilo I, Creech M, Gross B, et al (2007) Integration of biological networks and gene expression data using Cytoscape. Nat Protoc **2:** 2366–2382

Clough SJ, Bent AF (1998) Floral dip: a simplified method for *Agrobacterium*-mediated transformation of *Arabidopsis thaliana*. Plant J **16:** 735–743

Coles JP, Phillips AL, Croker SJ, García-Lepe R, Lewis MJ, Hedden P (1999) Modification of gibberellin production and plant development in *Arabidopsis* by sense and antisense expression of gibberellin 20-oxidase genes. Plant J **17:** 547–556

De Bruyne L, Höfte M, De Vleesschauwer D (2014) Connecting growth and defense: the emerging roles of brassinosteroids and gibberellins in plant innate immunity. Mol Plant **7:** 943–959

Dhondt S, Van Haerenborgh D, Van Cauwenbergh C, Merks RMH, Philips W, Beemster GTS, Inzé D (2012) Quantitative analysis of venation patterns of Arabidopsis leaves by supervised image analysis. Plant J **69:** 553–563

Dowell RD, Ryan O, Jansen A, Cheung D, Agarwala S, Danford T, Bernstein DA, Rolfe PA, Heisler LE, Chin B, et al (2010) Genotype to phenotype: a complex problem. Science **328:** 469

Félix M-A (2007) Cryptic quantitative evolution of the vulva intercellular signaling network in *Caenorhabditis*. Curr Biol **17:** 103–114

Félix M-A, Wagner A (2008) Robustness and evolution: concepts, insights and challenges from a developmental model system. Heredity (Edinb) **100:** 132–140

Gery C, Zuther E, Schulz E, Legoupi J, Chauveau A, McKhann H, Hincha DK, Téoulé E (2011) Natural variation in the freezing tolerance of *Arabidopsis thaliana*: effects of RNAi-induced CBF depletion and QTL localisation vary among accessions. Plant Sci **180:** 12–23

Goecks J, Nekrutenko A, Taylor J; Galaxy Team (2010) Galaxy: a comprehensive approach for supporting accessible, reproducible, and transparent computational research in the life sciences. Genome Biol **11:** R86

Gonzalez N, De Bodt S, Sulpice R, Jikumaru Y, Chae E, Dhondt S, Van Daele T, De Milde L, Weigel D, Kamiya Y, et al (2010) Increased leaf size: different means to an end. Plant Physiol **153:** 1261–1279

Gonzalez N, Vanhaeren H, Inzé D (2012) Leaf size control: complex coordination of cell division and expansion. Trends Plant Sci **17:** 332–340

Hedden P (2003) The genes of the Green Revolution. Trends Genet **19:** 5–9

Hedden P, Thomas SG (2012) Gibberellin biosynthesis and its regulation. Biochem J **444:** 11–25

Hepworth J, Lenhard M (2014) Regulation of plant lateral-organ growth by modulating cell number and size. Curr Opin Plant Biol **17:** 36–42

Howe EA, Sinha R, Schlauch D, Quackenbush J (2011) RNA-Seq analysis in MeV. Bioinformatics **27:** 3209–3210

Huang S, Raman AS, Ream JE, Fujiwara H, Cerny RE, Brown SM (1998) Overexpression of 20-oxidase confers a gibberellin-overproduction phenotype in Arabidopsis. Plant Physiol **118:** 773–781

Jiang Z, Xu G, Jing Y, Tang W, Lin R (2016) Phytochrome B and REVEILLE1/2-mediated signalling controls seed dormancy and germination in Arabidopsis. Nat Commun **7:** 12377

Kim JH, Choi D, Kende H (2003) The AtGRF family of putative transcription factors is involved in leaf and cotyledon growth in *Arabidopsis*. Plant J **36:** 94–104

Kojima M, Kamada-Nobusada T, Komatsu H, Takei K, Kuroha T, Mizutani M, Ashikari M, Ueguchi-Tanaka M, Matsuoka M, Suzuki K, Sakakibara H (2009) Highly sensitive and high-throughput analysis of plant hormones using MS-probe modification and liquid chromatography-tandem mass spectrometry: an application for hormone profiling in *Oryza sativa*. Plant Cell Physiol **50:** 1201–1214

Lenth RV, Hervé M (2014) lsmeans: Least-Squares Means. R package version 2.13, https://cran.r-project.org/web/packages/lsmeans/index.html

Li R, Li J, Li S, Qin G, Novák O, Pěnčík A, Ljung K, Aoyama T, Liu J, Murphy A, et al (2014) *ADP1* affects plant architecture by regulating local auxin biosynthesis. PLoS Genet **10:** e1003954

Nelissen H, Rymen B, Jikumaru Y, Demuynck K, Van Lijsebettens M, Kamiya Y, Inzé D, Beemster GTS (2012) A local maximum in gibberellin levels regulates maize leaf growth by spatial control of cell division. Curr Biol **22:** 1183–1187

North BV, Curtis D, Sham PC (2002) A note on the calculation of empirical *P* values from Monte Carlo procedures. Am J Hum Genet **71:** 439–441

Paaby AB, White AG, Riccardi DD, Gunsalus KC, Piano F, Rockman MV (2015) Wild worm embryogenesis harbors ubiquitous polygenic modifier variation. eLife **4:** e09178

Plackett ARG, Powers SJ, Fernandez-Garcia N, Urbanova T, Takebayashi Y, Seo M, Jikumaru Y, Benlloch R, Nilsson O, Ruiz-Rivero O, et al (2012) Analysis of the developmental roles of the *Arabidopsis* gibberellin 20-oxidases demonstrates that *GA20ox1,-2,* and *-3* are the dominant paralogs. Plant Cell **24:** 941–960

Ramšak Ž, Baebler Š, Rotter A, Korbar M, Mozetič I, Usadel B, Gruden K (2014) GoMapMan: integration, consolidation and visualization of plant gene annotations within the MapMan ontology. Nucleic Acids Res **42:** D1167–D1175

Rawat R, Schwartz J, Jones MA, Sairanen I, Cheng Y, Andersson CR, Zhao Y, Ljung K, Harmer SL (2009) REVEILLE1, a Myb-like transcription factor, integrates the circadian clock and auxin pathways. Proc Natl Acad Sci USA **106:** 16883–16888

R Core Team (2015) R: A Language and Environment for Statistical Computing. R Foundation for Statistical Computing, Vienna, Austria

Ribeiro DM, Araújo WL, Fernie AR, Schippers JH, Mueller-Roeber B (2012) Translatome and metabolome effects triggered by gibberellins during rosette growth in *Arabidopsis*. J Exp Bot **63:** 2769–2786

Rieu I, Ruiz-Rivero O, Fernandez-Garcia N, Griffiths J, Powers SJ, Gong F, Linhartova T, Eriksson S, Nilsson O, Thomas SG, et al (2008) The gibberellin biosynthetic genes *AtGA20ox1* and *AtGA20ox2* act, partially redundantly, to promote growth and development throughout the Arabidopsis life cycle. Plant J **53:** 488–504

Schilsky RL (2010) Personalized medicine in oncology: the future is now. Nat Rev Drug Discov **9:** 363–366

Schwechheimer C, Willige BC (2009) Shedding light on gibberellic acid signalling. Curr Opin Plant Biol **12:** 57–62

Shimada TL, Shimada T, Hara-Nishimura I (2010) A rapid and non-destructive screenable marker, FAST, for identifying transformed seeds of *Arabidopsis thaliana*. Plant J **61:** 519–528

Shinozaki Y, Hao S, Kojima M, Sakakibara H, Ozeki-Iida Y, Zheng Y, Fei Z, Zhong S, Giovannoni JJ, Rose JKC, et al (2015) Ethylene suppresses tomato (*Solanum lycopersicum*) fruit set through modification of gibberellin metabolism. Plant J **83:** 237–251

Ueguchi-Tanaka M, Nakajima M, Motoyuki A, Matsuoka M (2007) Gibberellin receptor and its role in gibberellin signaling in plants. Annu Rev Plant Biol **58:** 183–198

Van der Auwera GA, Carneiro MO, Chris Hartl C, Poplin R, del Angel G, Levy-Moonshine A, Jordan T, Shakir K, Roazen D, Thibault J, et al (2013) From FastQ data to high confidence variant calls: the Genome Analysis Toolkit best practices pipeline Curr Protoc Bioinformatics **11:** 11.10.1–11.10.33

Vanhaeren H, Gonzalez N, Coppens F, De Milde L, Van Daele T, Vermeersch M, Eloy NB, Storme V, Inzé D (2014) Combining growth-promoting genes leads to positive epistasis in *Arabidopsis thaliana*. eLife **3:** e02252

Vercruyssen L, Verkest A, Gonzalez N, Heyndrickx KS, Eeckhout D, Han S-K, Jégu T, Archacki R, Van Leene J, Andriankaja M, et al (2014) ANGUSTIFOLIA3 binds to SWI/SNF chromatin remodeling complexes to regulate transcription during *Arabidopsis* leaf development. Plant Cell **26:** 210–229

Vu V, Verster AJ, Schertzberg M, Chuluunbaatar T, Spensley M, Pajkic D, Hart GT, Moffat J, Fraser AG (2015) Natural variation in gene expression modulates the severity of mutant phenotypes. Cell **162:** 391–402

Weiss D, Ori N (2007) Mechanisms of cross talk between gibberellin and other hormones. Plant Physiol **144:** 1240–1246

Wu TD, Nacu S (2010) Fast and SNP-tolerant detection of complex variants and splicing in short reads. Bioinformatics **26:** 873–881

Zentella R, Zhang ZL, Park M, Thomas SG, Endo A, Murase K, Fleet CM, Jikumaru Y, Nambara E, Kamiya Y, Sun TP (2007) Global analysis of della direct targets in early gibberellin signaling in Arabidopsis. Plant Cell **19:** 3037–3057

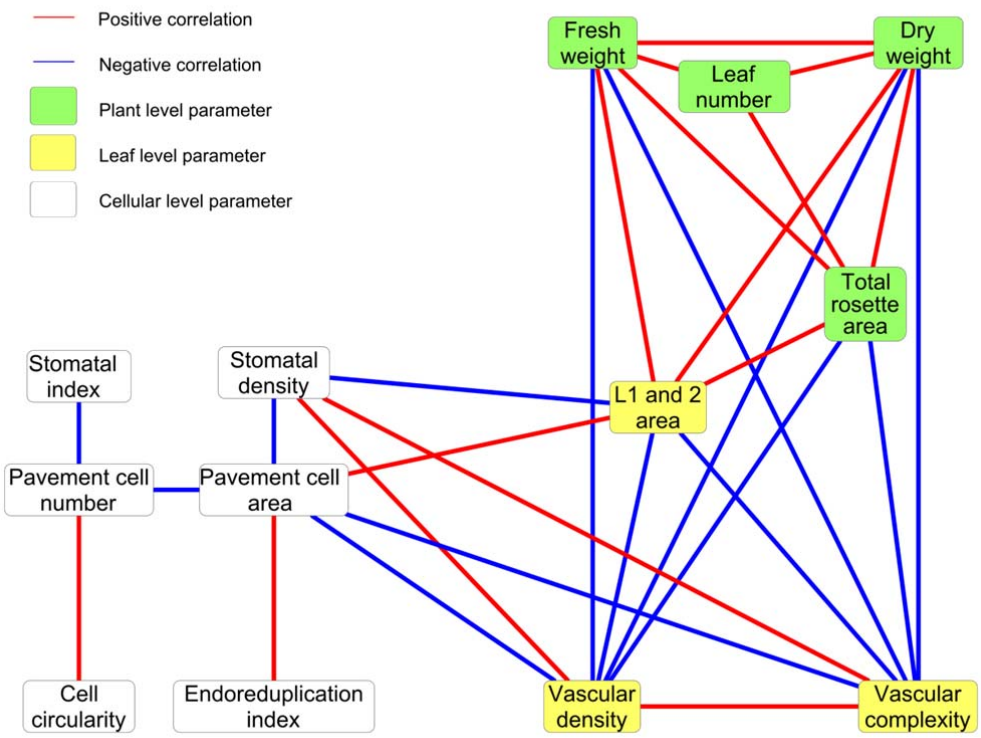

Supplemental Figure S1. Correlation between the shoot-related phenotypic measurements of the 17 Arabidopsis accessions. The parameters measured are fresh and dry weight; total rosette area; total number and area of leaves; pavement cell number, area, and circularity; endoreduplication index; stomatal density and index; vascular complexity and density of the first leaf pair. The green, yellow, and white nodes represent the parameters at plant, leaf, and cellular level, respectively. The cellular level parameters were measured from leaf 1 and 2. The red and blue edges show positive (correlation coefficient > 0.6) and negative correlation (correlation coefficient < -0.6) between parameters, respectively (adj-P value < 0.05).

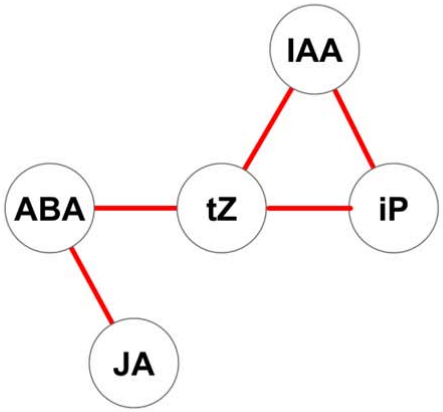

Supplemental Figure S2. Correlation between four of the major bioactive hormones (ABA, cytokinins, JA, and ABA) in 17 Arabidopsis accessions. The edges indicate a positive correlation (correlation coefficient > 0.6) between the hormones (adj-P value < 0.05).

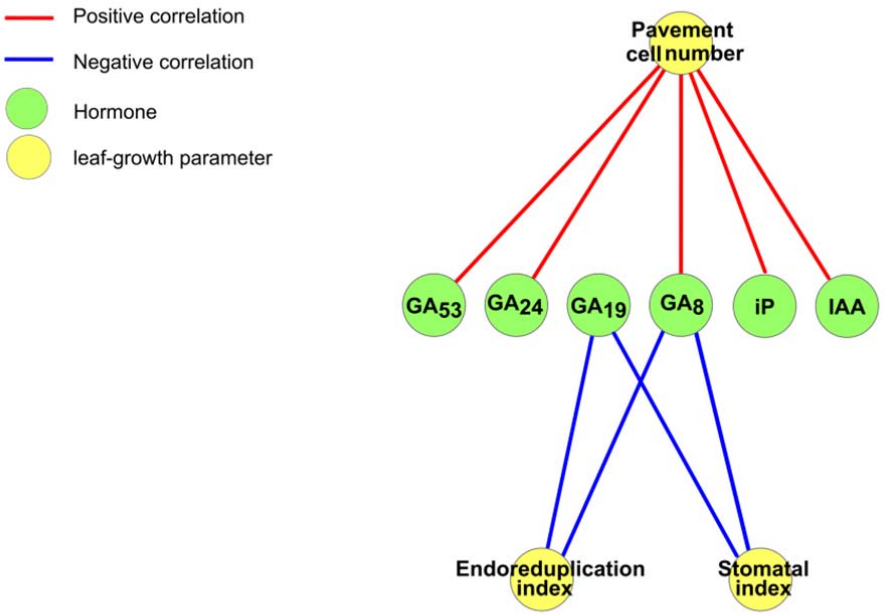

Supplemental Figure S3. Correlation between the leaf size-related parameters and hormones in the 17 Arabidopsis accessions. The red and blue edges show positive (correlation coefficient > 0.6) and negative correlation (correlation coefficient < -0.6) between parameters, respectively (adj-P value < 0.05).

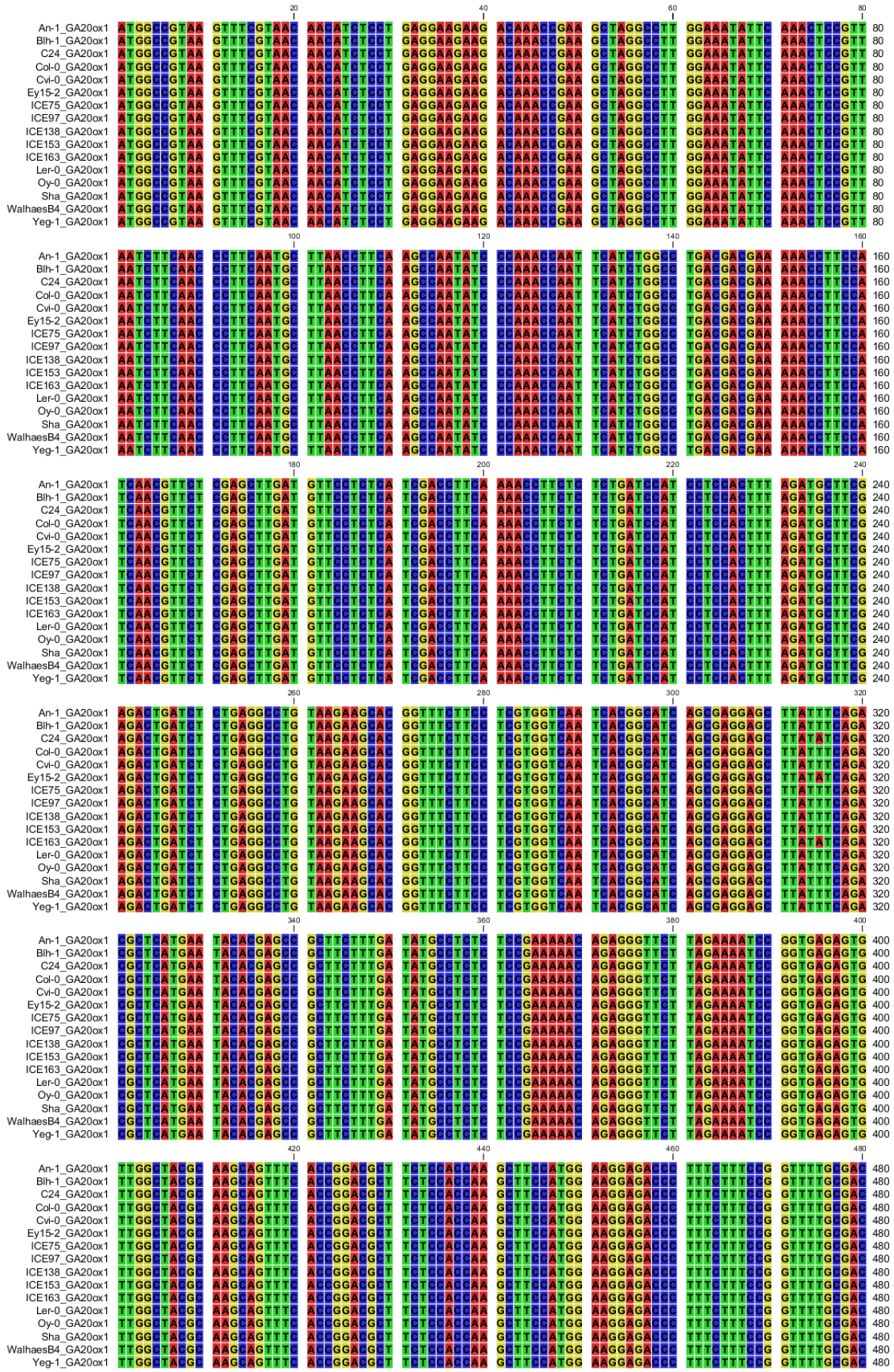
An-1_GA20ox1
Blh-1_GA20ox1
C24_GA20ox1
Col-0_GA20ox1
Cvi-0_GA20ox1
Ey15-2_GA20ox1
ICE75_GA20ox1
ICE97_GA20ox1
ICE138_GA20ox1
ICE153_GA20ox1
ICE163_GA20ox1
Ler-0_GA20ox1
Oy-0_GA20ox1
Sha_GA20ox1
WalhaesB4_GA20ox1
Yeg-1_GA20ox1

A

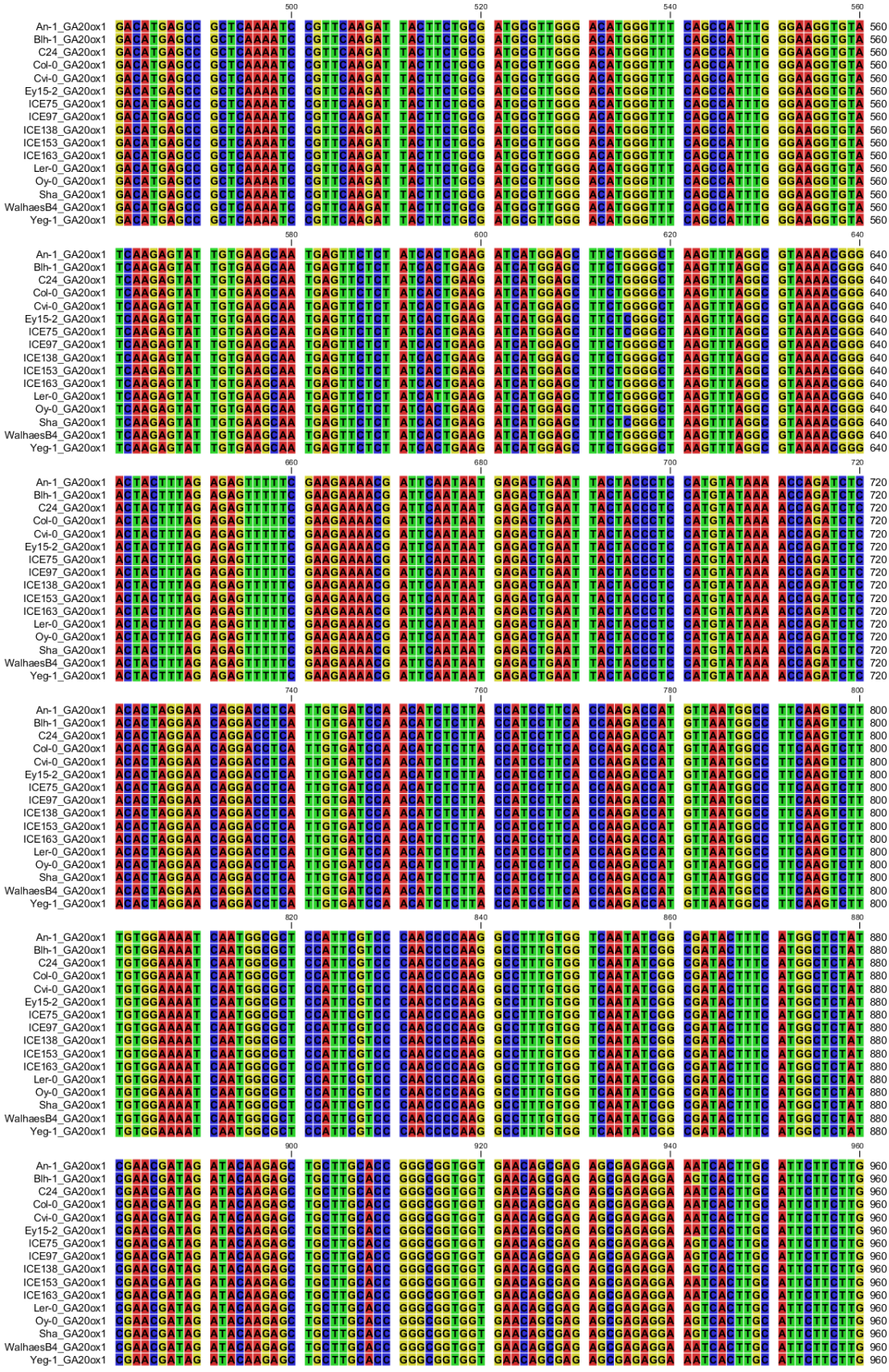
An-1_GA20ox1
Blh-1_GA20ox1
C24_GA20ox1
Col-0_GA20ox1
Cvi-0_GA20ox1
Ey15-2_GA20ox1
ICE75_GA20ox1
ICE97_GA20ox1
ICE138_GA20ox1
ICE153_GA20ox1
ICE163_GA20ox1
Ler-0_GA20ox1
Oy-0_GA20ox1
Sha_GA20ox1
WalhaesB4_GA20ox1
Yeg-1_GA20ox1

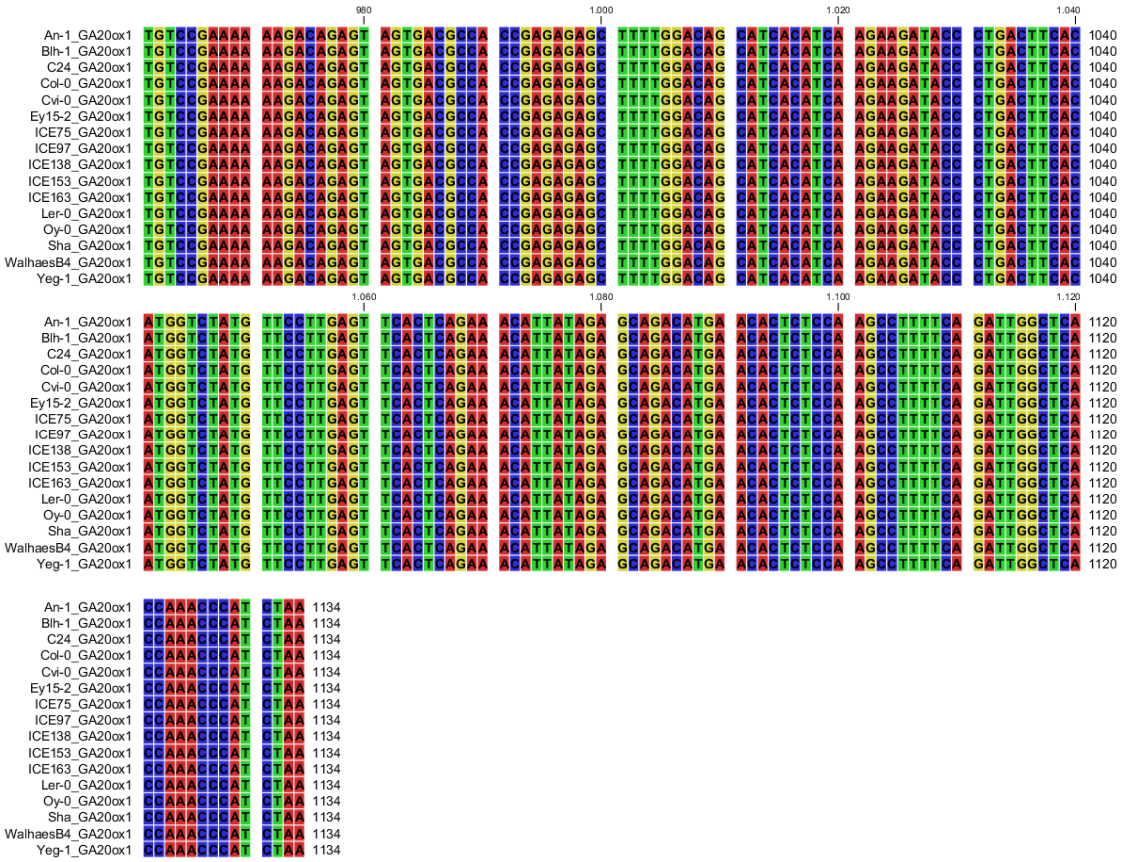
980
1.000
1.020
1.040
An-1_GA20ox1 TGTCCGAAAA AAGACAGAGT AGTGACGCCA CCGAGAGAGC TTTTGGACAG CATCACATCA AGAAGATACC CTGACTTCAC 1040
Bln-1_GA20ox1 TGTCCGAAAA AAGACAGAGT AGTGACGCCA CCGAGAGAGC TTTTGGACAG CATCACATCA AGAAGATACC CTGACTTCAC 1040
C24_GA20ox1 TGTCCGAAAA AAGACAGAGT AGTGACGCCA CCGAGAGAGC TTTTGGACAG CATCACATCA AGAAGATACC CTGACTTCAC 1040
Col-0_GA20ox1 TGTCCGAAAA AAGACAGAGT AGTGACGCCA CCGAGAGAGC TTTTGGACAG CATCACATCA AGAAGATACC CTGACTTCAC 1040
Cvi-0_GA20ox1 TGTCCGAAAA AAGACAGAGT AGTGACGCCA CCGAGAGAGC TTTTGGACAG CATCACATCA AGAAGATACC CTGACTTCAC 1040
Ey15-2_GA20ox1 TGTCCGAAAA AAGACAGAGT AGTGACGCCA CCGAGAGAGC TTTTGGACAG CATCACATCA AGAAGATACC CTGACTTCAC 1040
ICE75_GA20ox1 TGTCCGAAAA AAGACAGAGT AGTGACGCCA CCGAGAGAGC TTTTGGACAG CATCACATCA AGAAGATACC CTGACTTCAC 1040
ICE97_GA20ox1 TGTCCGAAAA AAGACAGAGT AGTGACGCCA CCGAGAGAGC TTTTGGACAG CATCACATCA AGAAGATACC CTGACTTCAC 1040
ICE138_GA20ox1 TGTCCGAAAA AAGACAGAGT AGTGACGCCA CCGAGAGAGC TTTTGGACAG CATCACATCA AGAAGATACC CTGACTTCAC 1040
ICE153_GA20ox1 TGTCCGAAAA AAGACAGAGT AGTGACGCCA CCGAGAGAGC TTTTGGACAG CATCACATCA AGAAGATACC CTGACTTCAC 1040
ICE163_GA20ox1 TGTCCGAAAA AAGACAGAGT AGTGACGCCA CCGAGAGAGC TTTTGGACAG CATCACATCA AGAAGATACC CTGACTTCAC 1040
Ler-0_GA20ox1 TGTCCGAAAA AAGACAGAGT AGTGACGCCA CCGAGAGAGC TTTTGGACAG CATCACATCA AGAAGATACC CTGACTTCAC 1040
Oy-0_GA20ox1 TGTCCGAAAA AAGACAGAGT AGTGACGCCA CCGAGAGAGC TTTTGGACAG CATCACATCA AGAAGATACC CTGACTTCAC 1040
Sha_GA20ox1 TGTCCGAAAA AAGACAGAGT AGTGACGCCA CCGAGAGAGC TTTTGGACAG CATCACATCA AGAAGATACC CTGACTTCAC 1040
WalhaesB4_GA20ox1 TGTCCGAAAA AAGACAGAGT AGTGACGCCA CCGAGAGAGC TTTTGGACAG CATCACATCA AGAAGATACC CTGACTTCAC 1040
Yeg-1_GA20ox1 TGTCCGAAAA AAGACAGAGT AGTGACGCCA CCGAGAGAGC TTTTGGACAG CATCACATCA AGAAGATACC CTGACTTCAC 1040
1.060
1.080
1.100
1.120
An-1_GA20ox1 ATGGTCTATG TTCCTTGAGT TCACTCAGAA ACATTATAGA GCAGACATGA ACACTCTCCA AGCCTTTTCA GATTGGCTCA 1120
Bln-1_GA20ox1 ATGGTCTATG TTCCTTGAGT TCACTCAGAA ACATTATAGA GCAGACATGA ACACTCTCCA AGCCTTTTCA GATTGGCTCA 1120
C24_GA20ox1 ATGGTCTATG TTCCTTGAGT TCACTCAGAA ACATTATAGA GCAGACATGA ACACTCTCCA AGCCTTTTCA GATTGGCTCA 1120
Col-0_GA20ox1 ATGGTCTATG TTCCTTGAGT TCACTCAGAA ACATTATAGA GCAGACATGA ACACTCTCCA AGCCTTTTCA GATTGGCTCA 1120
Cvi-0_GA20ox1 ATGGTCTATG TTCCTTGAGT TCACTCAGAA ACATTATAGA GCAGACATGA ACACTCTCCA AGCCTTTTCA GATTGGCTCA 1120
Ey15-2_GA20ox1 ATGGTCTATG TTCCTTGAGT TCACTCAGAA ACATTATAGA GCAGACATGA ACACTCTCCA AGCCTTTTCA GATTGGCTCA 1120
ICE75_GA20ox1 ATGGTCTATG TTCCTTGAGT TCACTCAGAA ACATTATAGA GCAGACATGA ACACTCTCCA AGCCTTTTCA GATTGGCTCA 1120
ICE97_GA20ox1 ATGGTCTATG TTCCTTGAGT TCACTCAGAA ACATTATAGA GCAGACATGA ACACTCTCCA AGCCTTTTCA GATTGGCTCA 1120
ICE138_GA20ox1 ATGGTCTATG TTCCTTGAGT TCACTCAGAA ACATTATAGA GCAGACATGA ACACTCTCCA AGCCTTTTCA GATTGGCTCA 1120
ICE153_GA20ox1 ATGGTCTATG TTCCTTGAGT TCACTCAGAA ACATTATAGA GCAGACATGA ACACTCTCCA AGCCTTTTCA GATTGGCTCA 1120
ICE163_GA20ox1 ATGGTCTATG TTCCTTGAGT TCACTCAGAA ACATTATAGA GCAGACATGA ACACTCTCCA AGCCTTTTCA GATTGGCTCA 1120
Ler-0_GA20ox1 ATGGTCTATG TTCCTTGAGT TCACTCAGAA ACATTATAGA GCAGACATGA ACACTCTCCA AGCCTTTTCA GATTGGCTCA 1120
Oy-0_GA20ox1 ATGGTCTATG TTCCTTGAGT TCACTCAGAA ACATTATAGA GCAGACATGA ACACTCTCCA AGCCTTTTCA GATTGGCTCA 1120
Sha_GA20ox1 ATGGTCTATG TTCCTTGAGT TCACTCAGAA ACATTATAGA GCAGACATGA ACACTCTCCA AGCCTTTTCA GATTGGCTCA 1120
WalhaesB4_GA20ox1 ATGGTCTATG TTCCTTGAGT TCACTCAGAA ACATTATAGA GCAGACATGA ACACTCTCCA AGCCTTTTCA GATTGGCTCA 1120
Yeg-1_GA20ox1 ATGGTCTATG TTCCTTGAGT TCACTCAGAA ACATTATAGA GCAGACATGA ACACTCTCCA AGCCTTTTCA GATTGGCTCA 1120
An-1_GA20ox1 CCAAACCCAT CTAA 1134
Bln-1_GA20ox1 CCAAACCCAT CTAA 1134
C24_GA20ox1 CCAAACCCAT CTAA 1134
Col-0_GA20ox1 CCAAACCCAT CTAA 1134
Cvi-0_GA20ox1 CCAAACCCAT CTAA 1134
Ey15-2_GA20ox1 CCAAACCCAT CTAA 1134
ICE75_GA20ox1 CCAAACCCAT CTAA 1134
ICE97_GA20ox1 CCAAACCCAT CTAA 1134
ICE138_GA20ox1 CCAAACCCAT CTAA 1134
ICE153_GA20ox1 CCAAACCCAT CTAA 1134
ICE163_GA20ox1 CCAAACCCAT CTAA 1134
Ler-0_GA20ox1 CCAAACCCAT CTAA 1134
Oy-0_GA20ox1 CCAAACCCAT CTAA 1134
Sha_GA20ox1 CCAAACCCAT CTAA 1134
WalhaesB4_GA20ox1 CCAAACCCAT CTAA 1134
Yeg-1_GA20ox1 CCAAACCCAT CTAA 1134

B

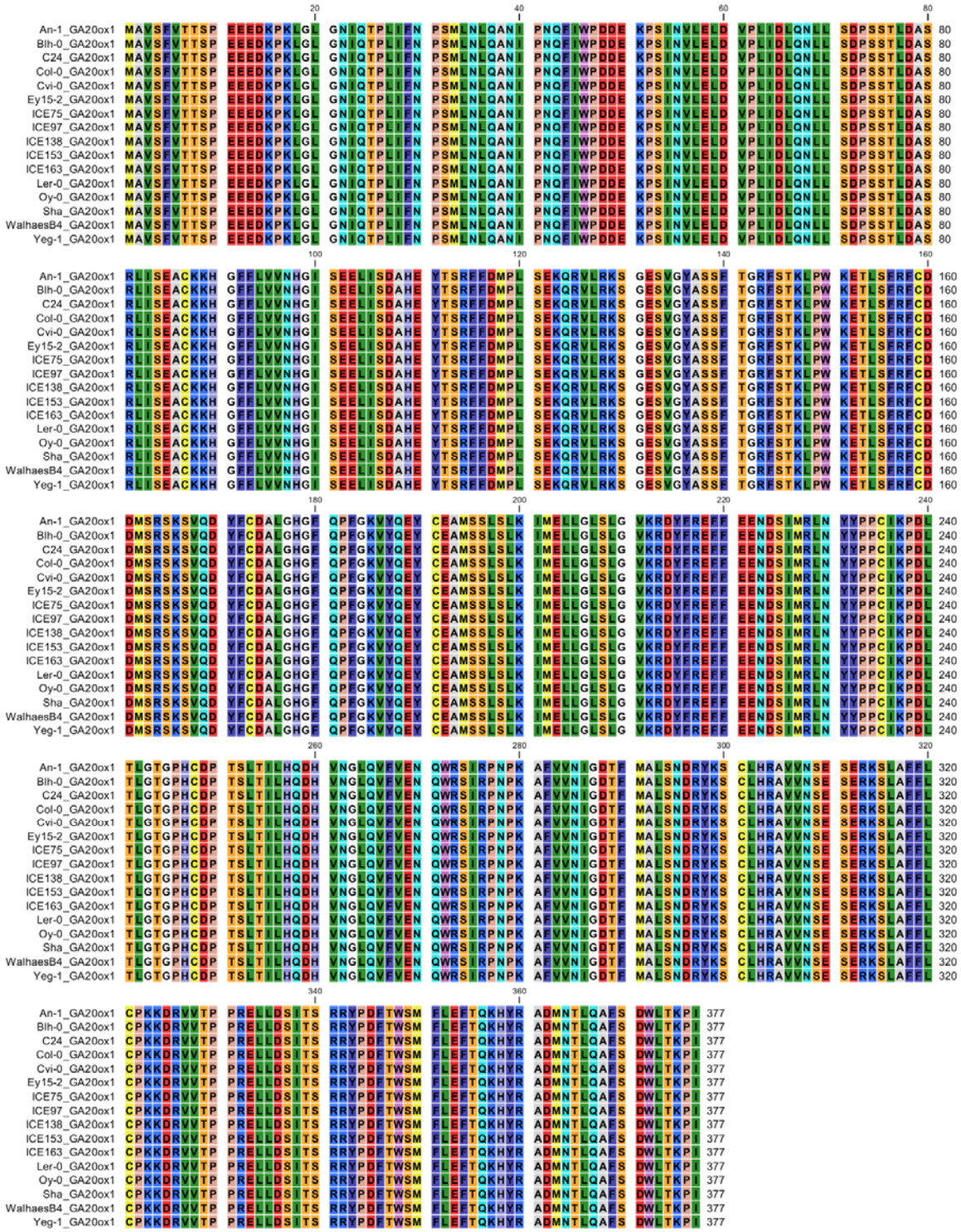

Supplemental Figure S4. Sequence alignments of *GA20ox1* cDNA (A) and the corresponding protein (B) from 16 of the 17 *Arabidopsis* accessions studied.

	cot	L1 and 2	L3	L4	L5	L6	L7	L8	L9	L10	L11	L12	L13	L14	L15	L16	L17	L18	L19
ICE61_E1	110	131	128	124	121	136	139	145	154	143	149	146	125	116					
ICE61_E2	109	121	132	119	127	133	127	126	123	117	111	100	98	70					
ICE61_E3	105	116	125	120	124	129	129	125	132	117	105	100	87	71					
AN-1_E1	73	90	75	79	78														
AN-1_E2	73	79	75	77	73														
AN-1_E3	63	72	72	65	64														
AN-1_E4	82	92	79	81	78														
AN-1_E5	86	65	67	64	55														
CVI-0_E1	104	89	89	99	108	138	165	245	286	420									
CVI-0_E2	101	94	99	106	107	119	135	141	138	120									
CVI-0_E3	102	100	103	110	114	128	152	166	147	197									
LER-0_E1	82	80	77	77	90	96													
LER-0_E2	87	85	90	94	111	134													
LER-0_E3	62	66	67	64	78	87													
LER-0_E4	81	92	86	91	107	126													
LER-0_E5	78	81	86	89	99	113													
BLH-1_E1	94	99	100	104	92	90	101												
BLH-1_E2	90	90	82	93	94	100	112												
BLH-1_E3	97	112	103	107	99	102	110												
BLH-1_E4	89	103	92	92	90	84	84												
BLH-1_E5	84	89	84	93	87	97	109												
ICE138_E2	97	107	105	108	126	134	129	122	122	117	113	105							
ICE138_E3	89	103	108	113	133	148	159	138	162	157	145	162							
ICE97_E1	125	118	104	97	97	87	90	93	104	120	117	123	157	150					
ICE97_E2	105	105	111	109	122	120	139	158	180	270	338	397	561	531					
ICE97_E4	115	112	118	112	126	127	146	162	190	283	409	537	667	675					
EY152_E1	99	96	100	102	106	103	109	108	131	124									
EY152_E2	101	101	97	94	96	105	112	109	122	118									
EY152_E3	100	99	95	93	99	99	105	104	115	116									
EY152_E4	97	100	98	98	103	106	104	108	120	115									
EY152_E5	96	100	99	96	107	101	115	114	137	133									
C24_E1	82	87	92	97	107	98	104	102	109	83	70	65	52	44					
C24_E2	77	78	89	95	95	88	86	81	67	54	44	31	26	22					
C24_E3	66	77	90	92	94	97	94	91	80	61	58	36	28	23					
C24_E4	69	77	91	98	105	100	95	90	83	70	61	42	34	37					
C24_E5	82	94	93	100	104	102	98	89	83	69	52	38	32	35					
YEG1_E1	112	123	114	112	113	103	110	100	116	130	145	158	162	171	100				
YEG1_E2	88	109	96	102	98	90	93	97	110	123	107	108	121	116	91				
WALHASB4_E1	91	105	110	119	115	110	108	105	101	84	73								
WALHASB4_E2	73	81	90	90	102	83	66	53	33	29	21								
WALHASB4_E3	80	102	97	105	112	116	118	112	107	98	71								
WALHASB4_E5	90	102	104	106	117	119	114	118	113	104	96								
SHA_E1	82	76	91	91	110	122	141	147											
SHA_E3	98	90	100	102	118	139	161	179											
SHA_E4	99	88	91	90	103	121	138	173											
COL-0_E2	110	146	143	137	138	140	171												
COL-0_E3	63	119	117	115	127	112	138												
COL-0_E4	67	104	116	125	124	134	144												
ICE153_E1	91	97	98	98	103	111	101	111	110	106	112	87	81	81	97				
ICE153_E2	90	96	95	94	101	111	103	104	103	95	99	87	75	69	57				
ICE153_E3	90	95	99	96	104	113	108	115	112	112	113	92	91	75	76				
ICE153_E5	102	109	121	112	128	132	127	139	156	158	184	155	194	170	166				
ICE163_E1	83	107	102	100	102	114	119	138	131	146	148	125	147	143	136	136	145	134	113
ICE163_E2	105	116	110	111	121	135	148	159	158	168	158	156	151	156	146	127	159	140	146
ICE163_E3	74	87	88	87	104	107	108	105	90	91	82	66	67	58	59	57	46	46	45
ICE163_E4	72	86	85	93	102	112	120	123	124	116	112	99	93	88	81	95	96	98	82
ICE163_E5	82	97	103	106	117	138	141	145	138	137	141	120	119	115	112	115	116	98	98
OY-0_E1	101	98	95	101	108	117	128	135	138	152	180	177							
OY-0_E2	88	97	96	100	117	123	137	138	151	154	166	175							
OY-0_E3	94	91	90	95	104	114	126	133	153	155	204	208							
OY-0_E4	107	96	97	101	105	116	127	139	153	174	206	232							
ICE75_E1	107	93	99	97	107	118	147	177	200	286	304	324	374	321	238				
ICE75_E2	112	95	101	99	107	114	135	158	167	200	192	192	187	152	153				
ICE75_E3	104	91	97	94	104	110	136	160	170	222	197	214	208	181	222				
ICE75_E4	106	99	102	97	110	111	144	163	174	220	202	243	224	218	195				

65<	65-75	75-85	85-95	95-105	105-115	115-125	125-135	>135

Supplemental Figure S5: Heat map representing, per accession, the predicted percent difference in each leaf area between each independent *GA20ox1* OE lines and their corresponding wild type.

Accession	cot	L1	L2	L3	L4	L5	L6	L7	L8	L9	L10	L11	L12	L13	L14	L15
ICE61	89	116	113	87	83	104	99	120	150	164	178	173	179	208		
An1	65	71	72	64	60	68	69	70								
Cvi-0	99	100	101	90	99	106	119	151	198	200						
Ler0	81	77	94	72	75	77	91	133								
Blh1	98	88	95	86	76	81	73	76	115							
ICE138	87	110	77	87	87	100	115	140	156	158	408	3971				
ICE97	87	100	104	89	91	95	93	91	104	119	128	115	129	235		
Ey15-2	81	93	98	81	78	88	89	98	118	144	87	78	113	195		
C24	87	87	71	70	52	51	47	65	80	88	96	101	90	74		
Yeg1	102	90	100	83	86	88	83	95	121	146	176	152	132			
WalhaesB4	80	96	89	104	100	114	117	148	180	190	237	270	454			
Sha	91	96	91	80	74	81	101	113	155	208	176					
Col-0	104	103	110	83	88	91	92	103	112	141						
ICE153	95	86	101	89	99	99	105	99	100	107	116	93	93	120		
ICE163	90	90	78	89	89	91	102	103	127	151	149	151	149	165	81	54
Oy0	95	105	107	85	79	83	89	91	95	113	143	161	158	159	77	
ICE75	94	69	97	74	77	80	87	101	105	106	119	82	48	51		

65<	65-75	75-85	85-95	95-105	105-115	115-125	125-135	>135

Supplemental Figure S6. Heat map representing, per accession, the percent difference in each leaf area between plants sprayed with GA_3 (GA) and the control plants (Mock).

A

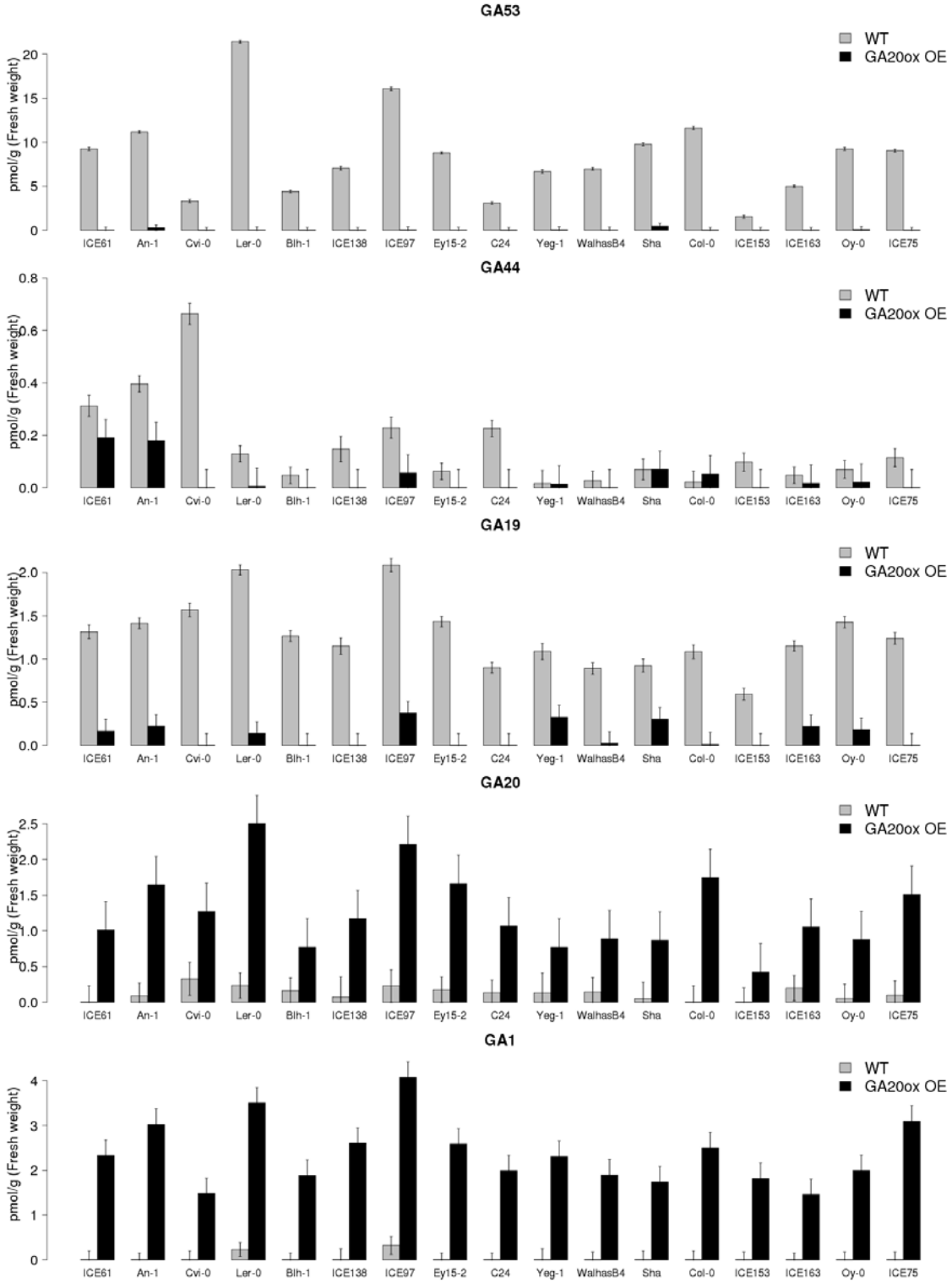
GA53
GA44
GA19
GA20
GA1
WT
GA20ox OE
pmol/g (Fresh weight)
ICE61
An-1
Cvi-0
Ler-0
Blh-1
ICE138
ICE97
Ey15-2
C24
Yeg-1
WalhasB4
Sha
Col-0
ICE153
ICE163
Oy-0
ICE75

B

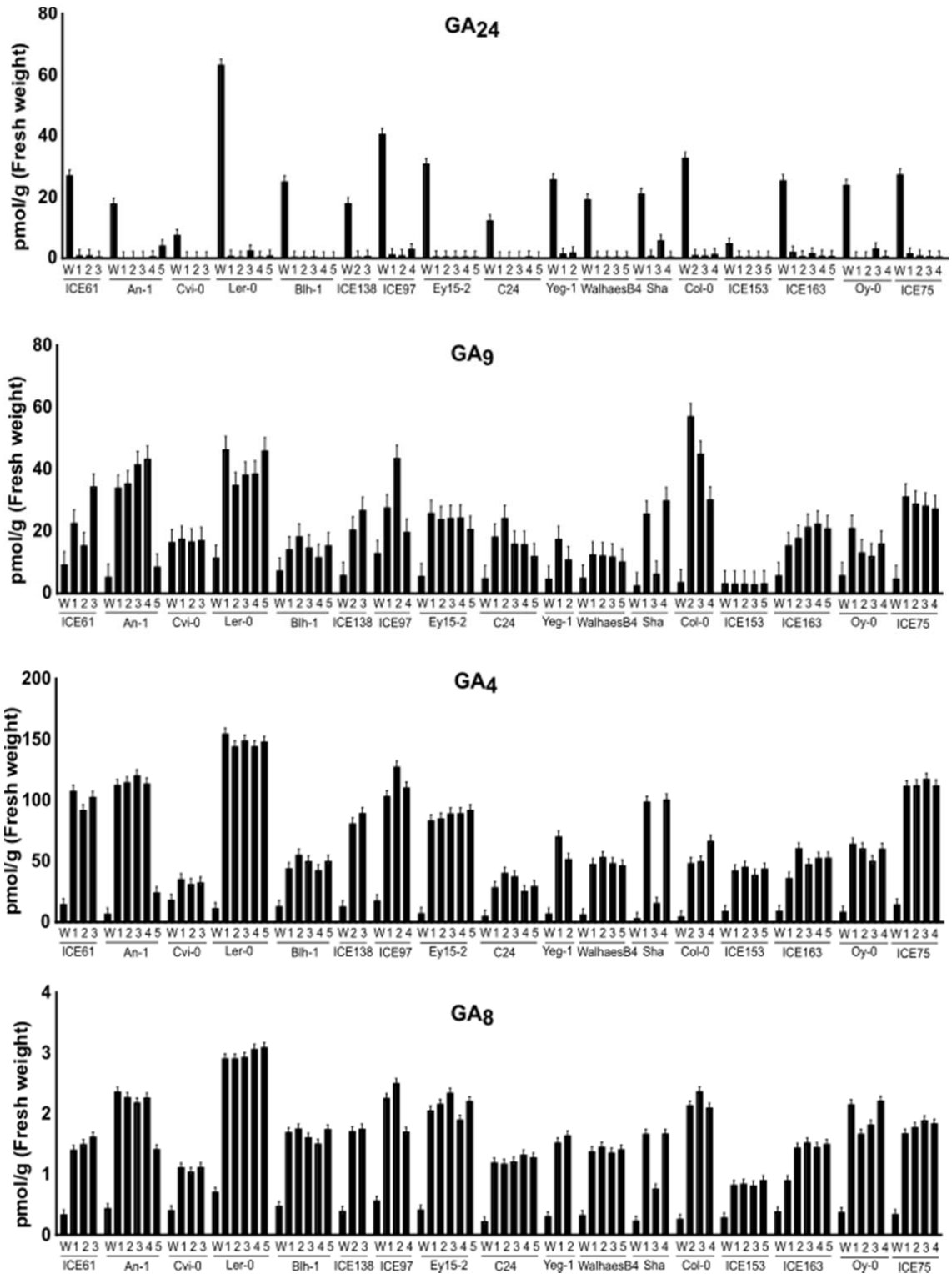
GA24
GA9
GA4
GA8
pmol/g (Fresh weight)
W1 2 3 ICE61
W1 2 3 4 5 An-1
W1 2 3 Cvi-0
W1 2 3 4 5 Ler-0
W1 2 3 4 5 Blh-1
W2 3 ICE138
W1 2 4 ICE97
W1 2 3 4 5 Ey15-2
W1 2 3 4 5 C24
W1 2 Yeg-1
W1 2 3 5 WalhaesB4
W1 3 4 Sha
W2 3 4 Col-0
W1 2 3 5 ICE153
W1 2 3 4 5 ICE163
W1 2 3 4 Oy-0
W1 2 3 4 ICE75

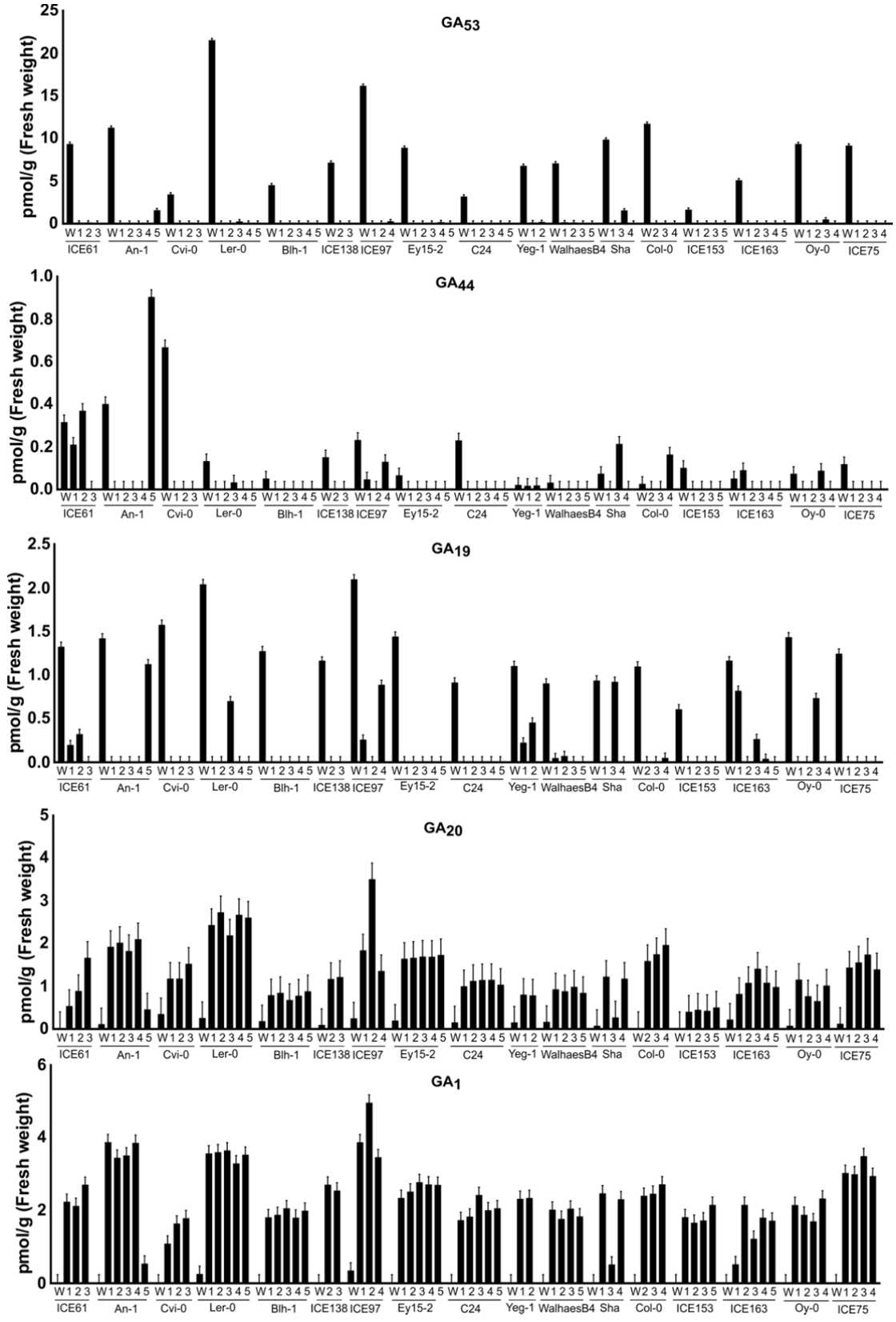

Supplemental Figure S7. GA levels in *GA20ox1* OE lines from the 17 Arabidopsis accessions. A. The normalized values represent the average concentrations between all transgenics for one accession and are represented with standard error bars. B. GA levels in individual *GA20ox1* OE lines. $GA_{24,}$ $GA_{9,}$ $GA_{4,}$ GA8,

GA_{53}, GA_{44}, GA_{19}, GA_{20} and GA_1 were measured from 12–day-old seedlings grown in soil. The normalized values are represented with standard error bars (N=3). W; wild type, 1-5; independent transgenic lines.

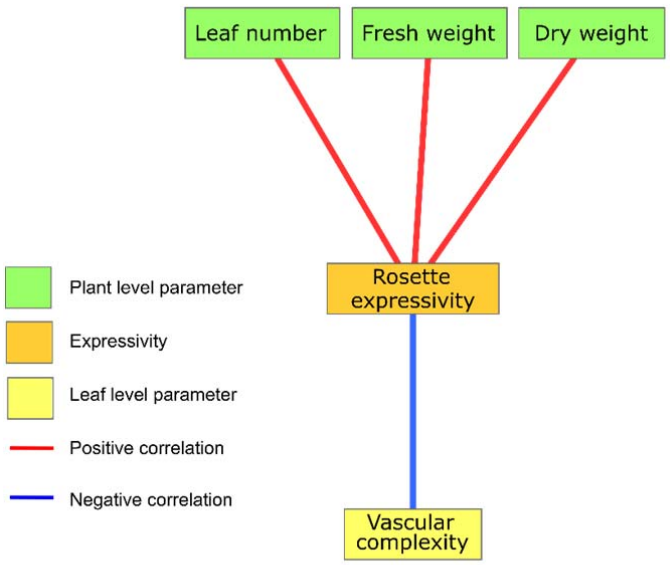

Supplemental Figure S8. Correlation analysis of phenotypic data. Correlation between phenotype parameters of wild types and expressivity of the *GA20ox1* OE effect in the transgenic lines. Node colours: green, plant level parameters; orange, expressivity; yellow, leaf level parameters. The red and blue edges show positive (correlation coefficient > 0.5) and negative correlation (correlation coefficient < -0.5) between parameters, respectively (adj-P value < 0.05).

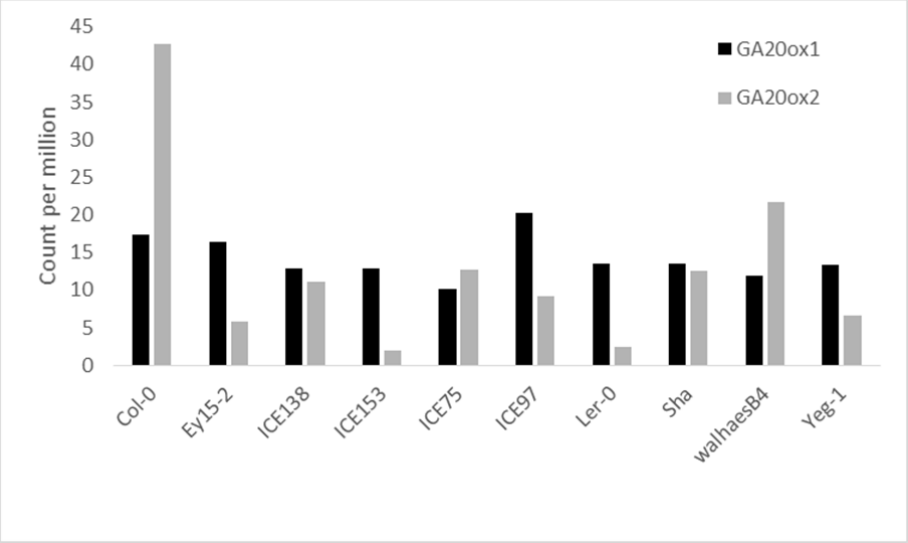

Supplemental Figure S9. *GA20ox1* and *GA20ox2* expression levels in the 10 Arabidopsis accessions used for RNAseq. Absolute values (count per million) are presented.

A

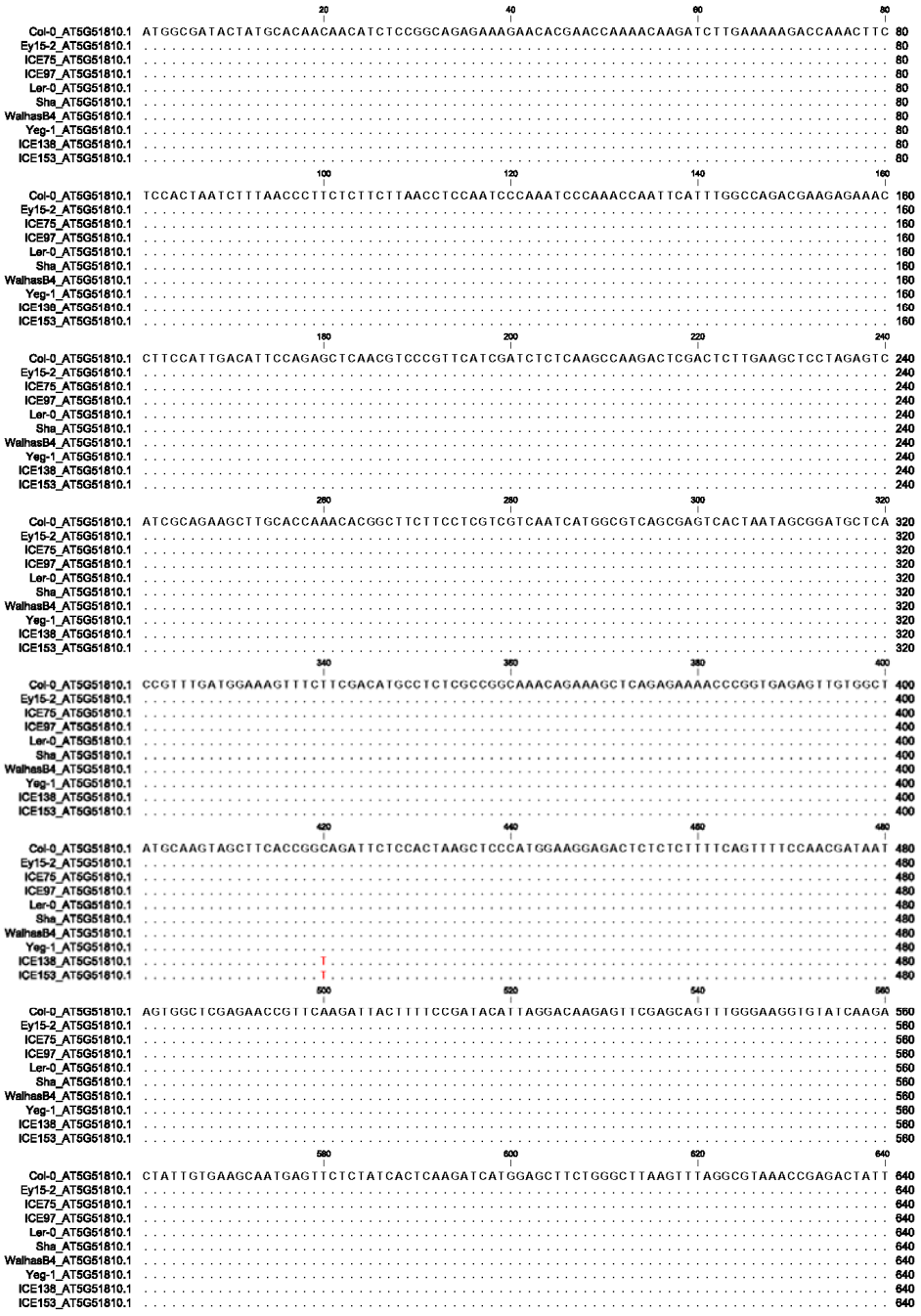
Col-0_AT5G51810.1 ATGGCGATACTATGCACAACAACATCTCCGGCAGAGAAAGAACACGAACCAAAACAAGATCTTGAAAAAGACCAAACTTC 80
Ey15-2_AT5G51810.1 80
ICE75_AT5G51810.1 80
ICE97_AT5G51810.1 80
Ler-0_AT5G51810.1 80
Sha_AT5G51810.1 80
WalhasB4_AT5G51810.1 80
Yeg-1_AT5G51810.1 80
ICE138_AT5G51810.1 80
ICE153_AT5G51810.1 80
Col-0_AT5G51810.1 TCCACTAATCTTTAACCCTTCTCTTCTTAACCTCCAATCCCAAATCCCAAACCAATTCATTTGGCCAGACGAAGAGAAAC 160
Ey15-2_AT5G51810.1 160
ICE75_AT5G51810.1 160
ICE97_AT5G51810.1 160
Ler-0_AT5G51810.1 160
Sha_AT5G51810.1 160
WalhasB4_AT5G51810.1 160
Yeg-1_AT5G51810.1 160
ICE138_AT5G51810.1 160
ICE153_AT5G51810.1 160
Col-0_AT5G51810.1 CTTCCATTGACATTCCAGAGCTCAACGTCCCGTTCATCGATCTCTCAAGCCAAGACTCGACTCTTGAAGCTCCTAGAGTC 240
Ey15-2_AT5G51810.1 240
ICE75_AT5G51810.1 240
ICE97_AT5G51810.1 240
Ler-0_AT5G51810.1 240
Sha_AT5G51810.1 240
WalhasB4_AT5G51810.1 240
Yeg-1_AT5G51810.1 240
ICE138_AT5G51810.1 240
ICE153_AT5G51810.1 240
Col-0_AT5G51810.1 ATCGCAGAAGCTTGCACCAAACACGGCTTCTTCCTCGTCGTCAATCATGGCGTCAGCGAGTCACTAATAGCGGATGCTCA 320
Ey15-2_AT5G51810.1 320
ICE75_AT5G51810.1 320
ICE97_AT5G51810.1 320
Ler-0_AT5G51810.1 320
Sha_AT5G51810.1 320
WalhasB4_AT5G51810.1 320
Yeg-1_AT5G51810.1 320
ICE138_AT5G51810.1 320
ICE153_AT5G51810.1 320
Col-0_AT5G51810.1 CCGTTTGATGGAAAGTTTCTTCGACATGCCTCTCGCCGGCAAACAGAAAGCTCAGAGAAAACCCGGTGAGAGTTGTGGCT 400
Ey15-2_AT5G51810.1 400
ICE75_AT5G51810.1 400
ICE97_AT5G51810.1 400
Ler-0_AT5G51810.1 400
Sha_AT5G51810.1 400
WalhasB4_AT5G51810.1 400
Yeg-1_AT5G51810.1 400
ICE138_AT5G51810.1 400
ICE153_AT5G51810.1 400
Col-0_AT5G51810.1 ATGCAAGTAGCTTCACCGGCAGATTCTCCACTAAGCTCCCATGGAAGGAGACTCTCTCTTTTCAGTTTTCCAACGATAAT 480
Ey15-2_AT5G51810.1 480
ICE75_AT5G51810.1 480
ICE97_AT5G51810.1 480
Ler-0_AT5G51810.1 480
Sha_AT5G51810.1 480
WalhasB4_AT5G51810.1 480
Yeg-1_AT5G51810.1 480
ICE138_AT5G51810.1 T 480
ICE153_AT5G51810.1 T 480
Col-0_AT5G51810.1 AGTGGCTCGAGAACCGTTCAAGATTACTTTTCCGATACATTAGGACAAGAGTTCGAGCAGTTTGGGAAGGTGTATCAAGA 560
Ey15-2_AT5G51810.1 560
ICE75_AT5G51810.1 560
ICE97_AT5G51810.1 560
Ler-0_AT5G51810.1 560
Sha_AT5G51810.1 560
WalhasB4_AT5G51810.1 560
Yeg-1_AT5G51810.1 560
ICE138_AT5G51810.1 560
ICE153_AT5G51810.1 560
Col-0_AT5G51810.1 CTATTGTGAAGCAATGAGTTCTCTATCACTCAAGATCATGGAGCTTCTGGGCTTAAGTTTAGGCGTAAACCGAGACTATT 640
Ey15-2_AT5G51810.1 640
ICE75_AT5G51810.1 640
ICE97_AT5G51810.1 640
Ler-0_AT5G51810.1 640
Sha_AT5G51810.1 640
WalhasB4_AT5G51810.1 640
Yeg-1_AT5G51810.1 640
ICE138_AT5G51810.1 640
ICE153_AT5G51810.1 640

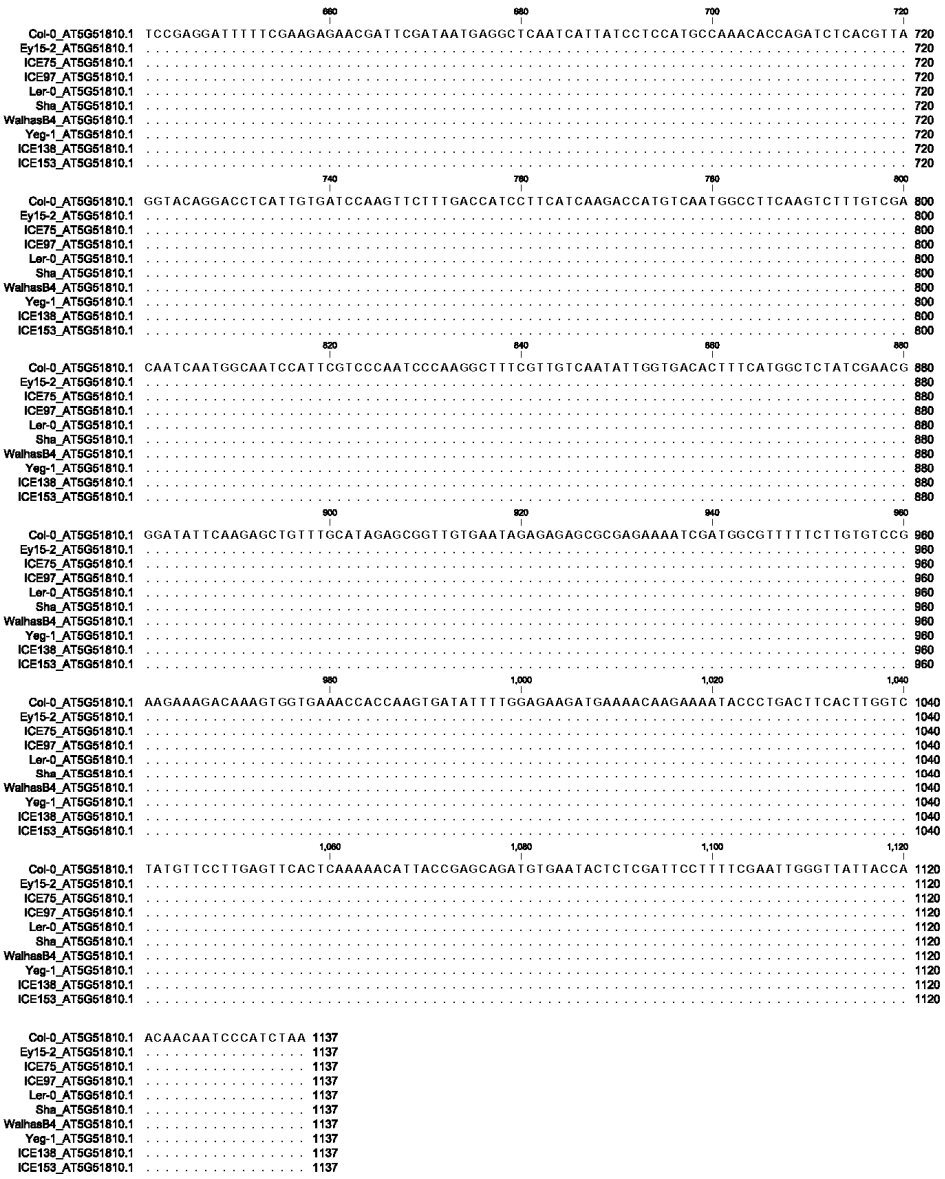
660 680 700 720
Col-0_AT5G51810.1 TCCGAGGATTTTTCGAAGAGAACGATTCGATAATGAGGCTCAATCATTATCCTCCATGCCAAACACCAGATCTCACGTTA 720
Ey15-2_AT5G51810.1 720
ICE75_AT5G51810.1 720
ICE97_AT5G51810.1 720
Ler-0_AT5G51810.1 720
Sha_AT5G51810.1 720
WalhasB4_AT5G51810.1 720
Yeg-1_AT5G51810.1 720
ICE138_AT5G51810.1 720
ICE153_AT5G51810.1 720
740 760 780 800
Col-0_AT5G51810.1 GGTACAGGACCTCATTGTGATCCAAGTTCTTTGACCATCCTTCATCAAGACCATGTCAATGGCCTTCAAGTCTTTGTCGA 800
Ey15-2_AT5G51810.1 800
ICE75_AT5G51810.1 800
ICE97_AT5G51810.1 800
Ler-0_AT5G51810.1 800
Sha_AT5G51810.1 800
WalhasB4_AT5G51810.1 800
Yeg-1_AT5G51810.1 800
ICE138_AT5G51810.1 800
ICE153_AT5G51810.1 800
820 840 860 880
Col-0_AT5G51810.1 CAATCAATGGCAATCCATTCGTCCCAATCCCAAGGCTTTCGTTGTCAATATTGGTGACACTTTCATGGCTCTATCGAACG 880
Ey15-2_AT5G51810.1 880
ICE75_AT5G51810.1 880
ICE97_AT5G51810.1 880
Ler-0_AT5G51810.1 880
Sha_AT5G51810.1 880
WalhasB4_AT5G51810.1 880
Yeg-1_AT5G51810.1 880
ICE138_AT5G51810.1 880
ICE153_AT5G51810.1 880
900 920 940 960
Col-0_AT5G51810.1 GGATATTCAAGAGCTGTTTGCATAGAGCGGTTGTGAATAGAGAGAGCGCGAGAAAATCGATGGCGTTTTTCTTGTGTCCG 960
Ey15-2_AT5G51810.1 960
ICE75_AT5G51810.1 960
ICE97_AT5G51810.1 960
Ler-0_AT5G51810.1 960
Sha_AT5G51810.1 960
WalhasB4_AT5G51810.1 960
Yeg-1_AT5G51810.1 960
ICE138_AT5G51810.1 960
ICE153_AT5G51810.1 960
980 1,000 1,020 1,040
Col-0_AT5G51810.1 AAGAAAGACAAAGTGGTGAAACCACCAAGTGATATTTTGGAGAAGATGAAAACAAGAAAATACCCTGACTTCACTTGGTC 1040
Ey15-2_AT5G51810.1 1040
ICE75_AT5G51810.1 1040
ICE97_AT5G51810.1 1040
Ler-0_AT5G51810.1 1040
Sha_AT5G51810.1 1040
WalhasB4_AT5G51810.1 1040
Yeg-1_AT5G51810.1 1040
ICE138_AT5G51810.1 1040
ICE153_AT5G51810.1 1040
1,060 1,080 1,100 1,120
Col-0_AT5G51810.1 TATGTTCCTTGAGTTCACTCAAAAACATTACCGAGCAGATGTGAATACTCTCGATTCCTTTTCGAATTGGGTTATTACCA 1120
Ey15-2_AT5G51810.1 1120
ICE75_AT5G51810.1 1120
ICE97_AT5G51810.1 1120
Ler-0_AT5G51810.1 1120
Sha_AT5G51810.1 1120
WalhasB4_AT5G51810.1 1120
Yeg-1_AT5G51810.1 1120
ICE138_AT5G51810.1 1120
ICE153_AT5G51810.1 1120
Col-0_AT5G51810.1 ACAACAATCCCATCTAA 1137
Ey15-2_AT5G51810.1 1137
ICE75_AT5G51810.1 1137
ICE97_AT5G51810.1 1137
Ler-0_AT5G51810.1 1137
Sha_AT5G51810.1 1137
WalhasB4_AT5G51810.1 1137
Yeg-1_AT5G51810.1 1137
ICE138_AT5G51810.1 1137
ICE153_AT5G51810.1 1137

B

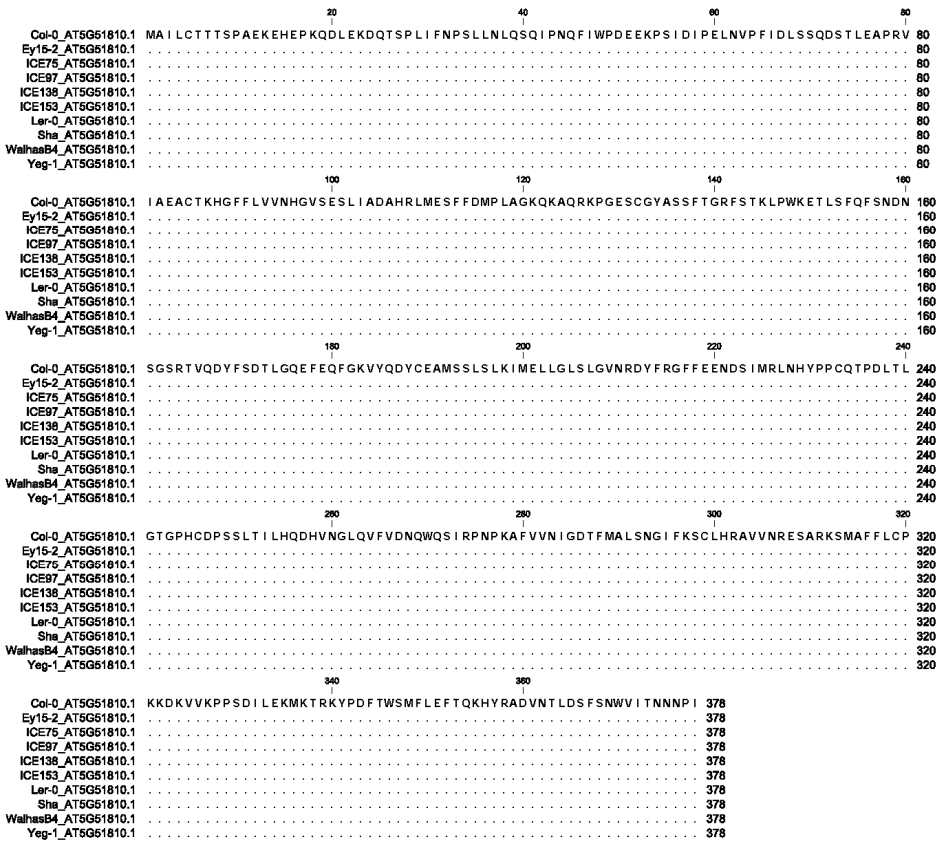

Supplemental Figure S10. Sequence alignments of *GA20ox2* cDNA (A) and the corresponding protein (B) from 10 of the 17 *Arabidopsis* accessions studied.

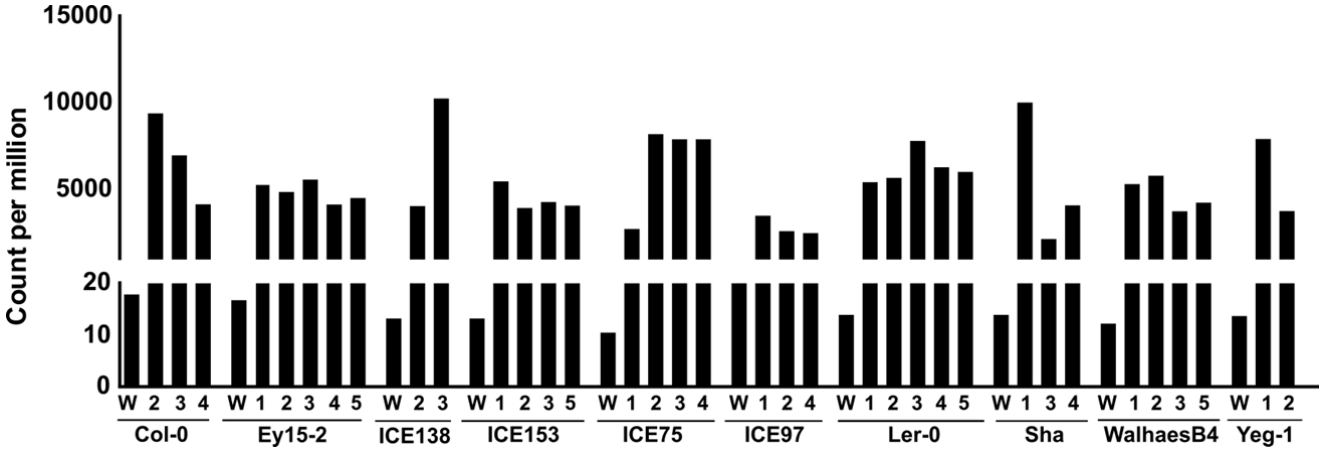

Supplemental Figure S11. *GA20ox1* expression level in the transgenic lines from 10 Arabidopsis accessions. Absolute value (count per million) of expression level of *GA20ox1* from RNA-Seq data in wild-type (W) and independent transgenic lines (1-5) of 10 accessions.

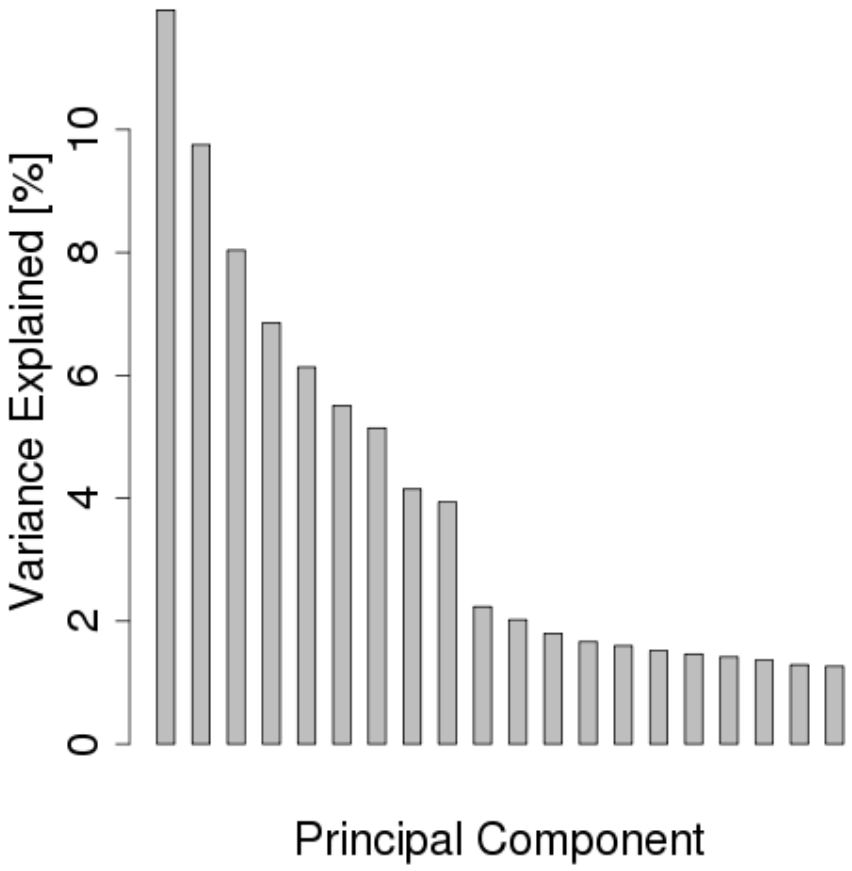

Supplemental Figure S12: Variance explained by first 20 components for th RNAseq analysis from the 10 accessions.

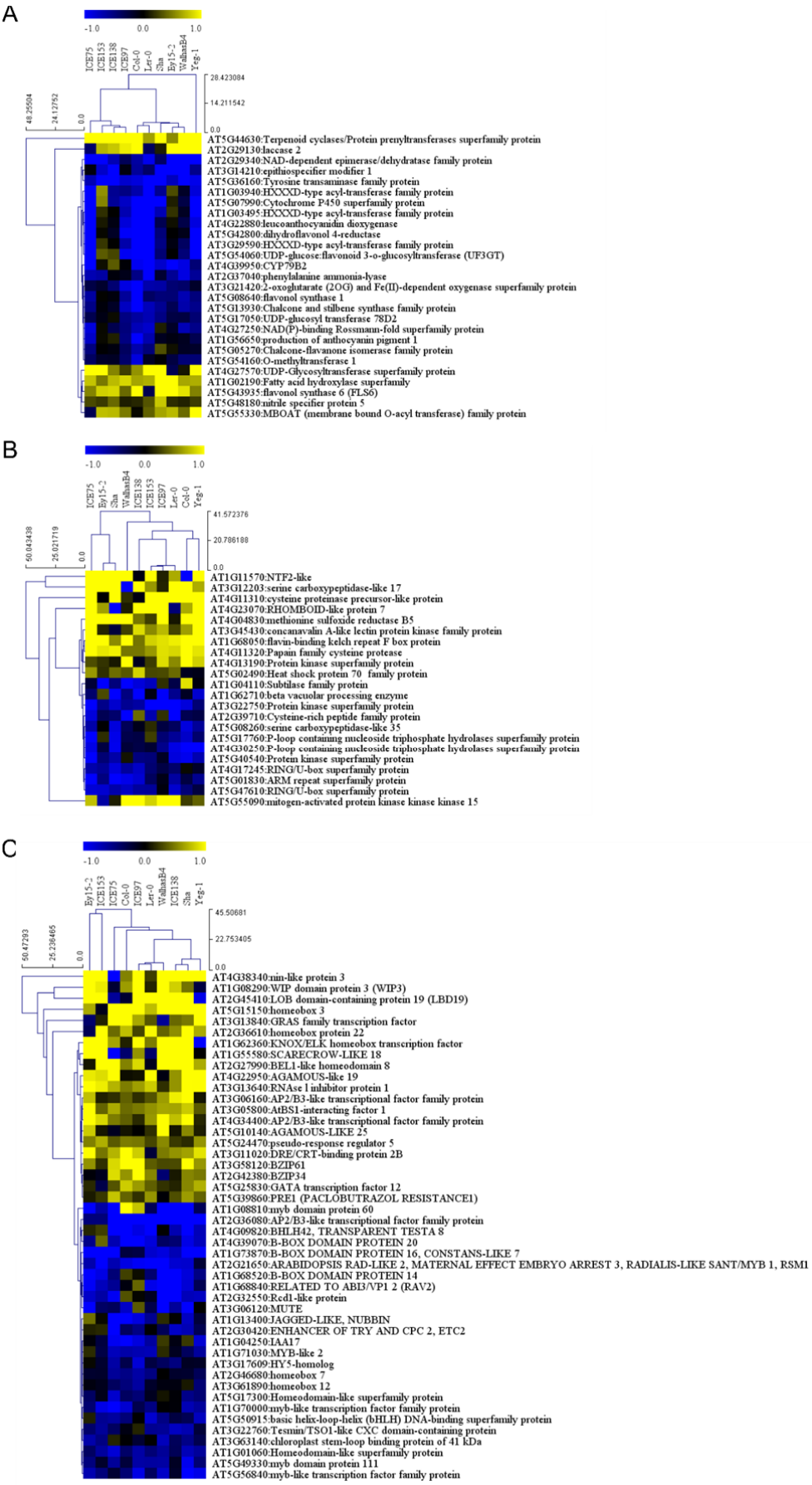
A
-1.0
0.0
1.0
ICE75
ICE153
ICE138
ICE97
Col-0
Ler-0
Sha
By15-2
WalhamB4
Yeg-1
28.423084
14.211542
0.0
48.25504
24.12752
0.0
AT5G44630:Terpenoid cyclases/Protein prenyltransferases superfamily protein
AT2G29130:laccase 2
AT2G29340:NAD-dependent epimerase/dehydratase family protein
AT3G14210:epithiospecifier modifier 1
AT5G36160:Tyrosine transaminase family protein
AT1G03940:HXXXD-type acyl-transferase family protein
AT5G07990:Cytochrome P450 superfamily protein
AT1G03495:HXXXD-type acyl-transferase family protein
AT4G22880:leucoanthocyanidin dioxygenase
AT5G42800:dihydroflavonol 4-reductase
AT3G29590:HXXXD-type acyl-transferase family protein
AT5G54060:UDP-glucose:flavonoid 3-o-glucosyltransferase (UF3GT)
AT4G39950:CYP79B2
AT2G37040:phenylalanine ammonia-lyase
AT3G21420:2-oxoglutarate (2OG) and Fe(II)-dependent oxygenase superfamily protein
AT5G08640:flavonol synthase 1
AT5G13930:Chalcone and stilbene synthase family protein
AT5G17050:UDP-glucosyl transferase 78D2
AT4G27250:NAD(P)-binding Rossmann-fold superfamily protein
AT1G56650:production of anthocyanin pigment 1
AT5G05270:Chalcone-flavanone isomerase family protein
AT5G54160:O-methyltransferase 1
AT4G27570:UDP-Glycosyltransferase superfamily protein
AT1G02190:Fatty acid hydroxylase superfamily
AT5G43935:flavonol synthase 6 (FLS6)
AT5G48180:nitrile specifier protein 5
AT5G55330:MBOAT (membrane bound O-acyl transferase) family protein
B
-1.0
0.0
1.0
ICE75
By15-2
Sha
WalhamB4
ICE138
ICE153
ICE97
Ler-0
Col-0
Yeg-1
41.572376
20.786188
0.0
50.043438
25.021719
0.0
AT1G11570:NTF2-like
AT3G12203:serine carboxypeptidase-like 17
AT4G11310:cysteine proteinase precursor-like protein
AT4G23070:RHOMBOID-like protein 7
AT4G04830:methionine sulfoxide reductase B5
AT3G45430:concanavalin A-like lectin protein kinase family protein
AT1G68050:flavin-binding kelch repeat F box protein
AT4G11320:Papain family cysteine protease
AT4G13190:Protein kinase superfamily protein
AT5G02490:Heat shock protein 70 family protein
AT1G04110:Subtilase family protein
AT1G62710:beta vacuolar processing enzyme
AT3G22750:Protein kinase superfamily protein
AT2G39710:Cysteine-rich peptide family protein
AT5G08260:serine carboxypeptidase-like 35
AT5G17760:P-loop containing nucleoside triphosphate hydrolases superfamily protein
AT4G30250:P-loop containing nucleoside triphosphate hydrolases superfamily protein
AT5G40540:Protein kinase superfamily protein
AT4G17245:RING/U-box superfamily protein
AT5G01830:ARM repeat superfamily protein
AT5G47610:RING/U-box superfamily protein
AT5G55090:mitogen-activated protein kinase kinase kinase 15
C
-1.0
0.0
1.0
By15-2
ICE153
ICE75
Col-0
ICE97
Ler-0
WalhamB4
ICE138
Sha
Yeg-1
45.50681
22.753405
0.0
50.47293
25.238465
0.0
AT4G38340:nin-like protein 3
AT1G08290:WIP domain protein 3 (WIP3)
AT2G45410:LOB domain-containing protein 19 (LBD19)
AT5G15150:homeobox 3
AT3G13840:GRAS family transcription factor
AT2G36610:homeobox protein 22
AT1G62360:KNOX/ELK homeobox transcription factor
AT1G55580:SCARECROW-LIKE 18
AT2G27990:BEL1-like homeodomain 8
AT4G22950:AGAMOUS-like 19
AT3G13640:RNAse l inhibitor protein 1
AT3G06160:AP2/B3-like transcriptional factor family protein
AT3G05800:AtBS1-interacting factor 1
AT4G34400:AP2/B3-like transcriptional factor family protein
AT5G10140:AGAMOUS-LIKE 25
AT5G24470:pseudo-response regulator 5
AT3G11020:DRE/CRT-binding protein 2B
AT3G58120:BZIP61
AT2G42380:BZIP34
AT5G25830:GATA transcription factor 12
AT5G39860:PRE1 (PACLOBUTRAZOL RESISTANCE1)
AT1G08810:myb domain protein 60
AT2G36080:AP2/B3-like transcriptional factor family protein
AT4G09820:BHLH42, TRANSPARENT TESTA 8
AT4G39070:B-BOX DOMAIN PROTEIN 20
AT1G73870:B-BOX DOMAIN PROTEIN 16, CONSTANS-LIKE 7
AT2G21650:ARABIDOPSIS RAD-LIKE 2, MATERNAL EFFECT EMBRYO ARREST 3, RADIALIS-LIKE SANT/MYB 1, RSM1
AT1G68520:B-BOX DOMAIN PROTEIN 14
AT1G68840:RELATED TO ABI3/VP1 2 (RAV2)
AT2G32550:Rcd1-like protein
AT3G06120:MUTE
AT1G13400:JAGGED-LIKE, NUBBIN
AT2G30420:ENHANCER OF TRY AND CPC 2, ETC2
AT1G04250:IAA17
AT1G71030:MYB-like 2
AT3G17609:HY5-homolog
AT2G46680:homeobox 7
AT3G61890:homeobox 12
AT5G17300:Homeodomain-like superfamily protein
AT1G70000:myb-like transcription factor family protein
AT5G50915:basic helix-loop-helix (bHLH) DNA-binding superfamily protein
AT3G22760:Tesmin/TSO1-like CXC domain-containing protein
AT3G63140:chloroplast stem-loop binding protein of 41 kDa
AT1G01060:Homeodomain-like superfamily protein
AT5G49330:myb domain protein 111
AT5G56840:myb-like transcription factor family protein

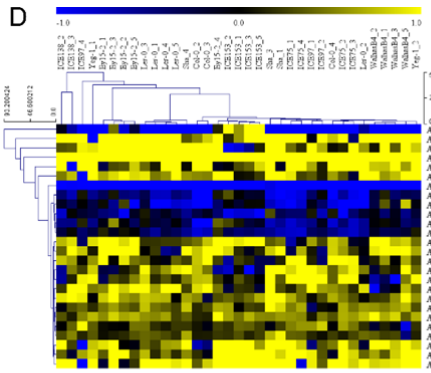
D
AT5G51810:gibberellin 20 oxidase 2
AT1G75590:small auxin upregulated RNA 52
AT3G03850:small auxin upregulated RNA 26
AT4G25420:gibberellin 20-oxidase 1
AT1G78440:gibberellin 2-oxidase 1
AT4G23340:2-oxoglutarate (2OG) and Fe(II)-dependent oxygenase superfamily protein
AT1G15550:gibberellin 3-oxidase 1
AT3G16450:jacalin-related lectin 33
AT2G31230:ethylene-responsive element binding factor 15
AT3G60690:SAUR-like auxin-responsive protein family
AT3G16460:jacalin-related lectin 34
AT5G05860:UDP-glucosyl transferase 76C2
AT1G30100:9-cis-epoxycarotenoid dioxygenase
AT2G42820:HVA22-like protein F
AT4G17500:ethylene responsive element binding factor 6
AT1G29500:SAUR-like auxin-responsive protein family
AT5G18030:small auxin upregulated RNA 21
AT1G29510:small auxin upregulated RNA 67
AT4G34800:small auxin upregulated RNA 4
AT1G19830:small auxin upregulated RNA 54
AT1G30040:gibberellin 2-oxidase2
AT2G17230:exordium like 5
AT5G48180:nitrile specifier protein 5
AT1G47990:gibberellin 2-oxidase 4
AT4G34790:small auxin upregulated RNA 3
AT5G56300:gibberellic acid methyltransferase 2

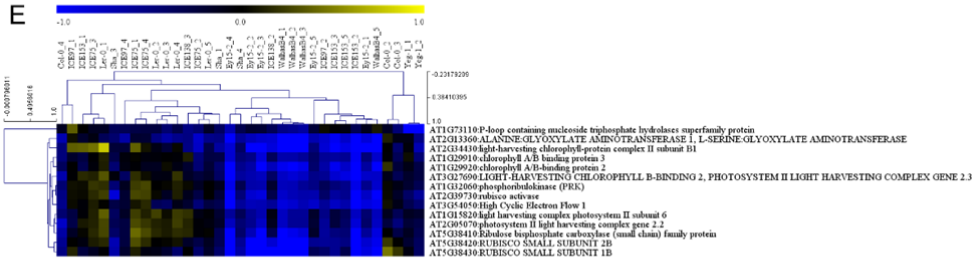
E
AT1G73110:P-loop containing nucleoside triphosphate hydrolases superfamily protein
AT2G13360:ALANINE:GLYOXYLATE AMINOTRANSFERASE 1, L-SERINE:GLYOXYLATE AMINOTRANSFERASE
AT2G34430:light-harvesting chlorophyll-protein complex II subunit B1
AT1G29910:chlorophyll A/B binding protein 3
AT1G29920:chlorophyll A/B-binding protein 2
AT3G27690:LIGHT-HARVESTING CHLOROPHYLL B-BINDING 2, PHOTOSYSTEM II LIGHT HARVESTING COMPLEX GENE 2.3
AT1G32060:phosphoribulokinase (PRK)
AT2G39730:rubisco activase
AT3G54050:High Cyclic Electron Flow 1
AT1G15820:light harvesting complex photosystem II subunit 6
AT2G05070:photosystem II light harvesting complex gene 2.2
AT5G38410:Ribulose bisphosphate carboxylase (small chain) family protein
AT5G38420:RUBISCO SMALL SUBUNIT 2B
AT5G38430:RUBISCO SMALL SUBUNIT 1B

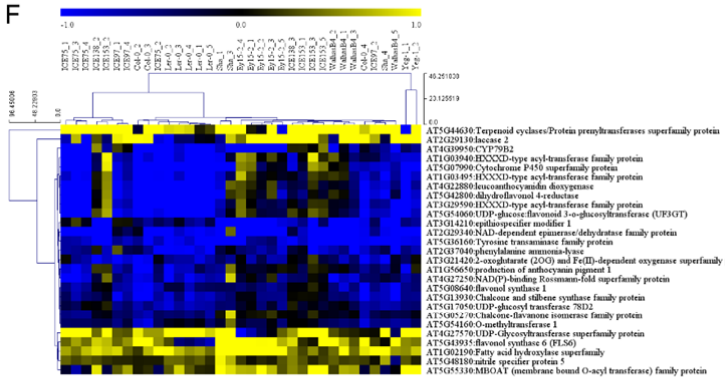
F
AT5G44630:Terpenoid cyclases/Protein prenyltransferases superfamily protein
AT2G29130:laccase 2
AT4G39950:CYP79B2
AT1G03940:HXXXD-type acyl-transferase family protein
AT5G07990:Cytochrome P450 superfamily protein
AT1G03495:HXXXD-type acyl-transferase family protein
AT4G22880:leucoanthocyanidin dioxygenase
AT5G42800:dihydroflavonol 4-reductase
AT3G29590:HXXXD-type acyl-transferase family protein
AT5G54060:UDP-glucose:flavonoid 3-o-glucosyltransferase (UF3GT)
AT3G14210:epithiospecifier modifier 1
AT2G29340:NAD-dependent epimerase/dehydratase family protein
AT5G36160:Tyrosine transaminase family protein
AT2G37040:phenylalanine ammonia-lyase
AT3G21420:2-oxoglutarate (2OG) and Fe(II)-dependent oxygenase superfamily protein
AT1G56650:production of anthocyanin pigment 1
AT4G27250:NAD(P)-binding Rossmann-fold superfamily protein
AT5G08640:flavonol synthase 1
AT5G13930:Chalcone and stilbene synthase family protein
AT5G17050:UDP-glucosyl transferase 78D2
AT5G05270:Chalcone-flavanone isomerase family protein
AT5G54160:O-methyltransferase 1
AT4G27570:UDP-Glycosyltransferase superfamily protein
AT5G41935:flavonol synthase 6 (FLS6)
AT1G02190:Fatty acid hydroxylase superfamily
AT5G48180:nitrile specifier protein 5
AT5G55330:MBOAT (membrane bound O-acyl transferase) family protein

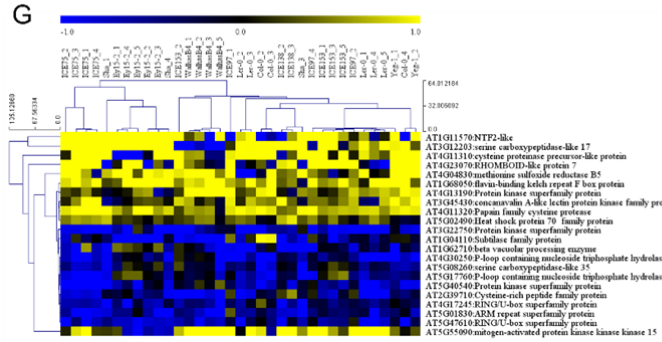
G
AT1G11570:NTF2-like
AT3G12203:serine carboxypeptidase-like 17
AT4G11310:cysteine proteinase precursor-like protein
AT4G23970:RHOMBOID-like protein 7
AT4G04830:methionine sulfoxide reductase B5
AT1G68050:flavin-binding kelch repeat F box protein
AT4G13190:Protein kinase superfamily protein
AT3G45410:concanavalin A-like lectin protein kinase family protein
AT4G11320:Papain family cysteine protease
AT5G02490:Heat shock protein 70 family protein
AT3G22750:Protein kinase superfamily protein
AT1G04110:Subtilase family protein
AT1G62710:beta vacuolar processing enzyme
AT4G30250:P-loop containing nucleoside triphosphate hydrolases superfamily protein
AT5G08260:serine carboxypeptidase-like 35
AT5G17760:P-loop containing nucleoside triphosphate hydrolases superfamily protein
AT5G40540:Protein kinase superfamily protein
AT2G39710:Cysteine-rich peptide family protein
AT4G17245:RING/U-box superfamily protein
AT5G01830:ARM repeat superfamily protein
AT5G47610:RING/U-box superfamily protein
AT5G55090:mitogen-activated protein kinase kinase kinase 15

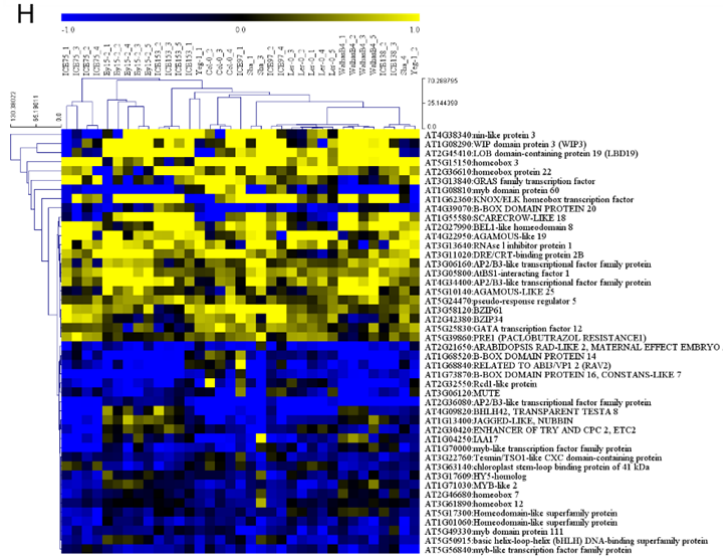
H
AT4G38340:nin-like protein 3
AT1G08290:WIP domain protein 3 (WIP3)
AT2G45410:LOB domain-containing protein 19 (LBD19)
AT5G01510:homeobox 3
AT2G36610:homeobox protein 22
AT3G13840:GRAS family transcription factor
AT1G08810:myb domain protein 60
AT1G62360:KNOX/ELK homeobox transcription factor
AT4G39070:B-BOX DOMAIN PROTEIN 20
AT1G55580:SCARECROW-LIKE 18
AT2G27990:BEL1-like homeodomain 8
AT4G22950:AGAMOUS-like 19
AT3G13640:RNAse 1 inhibitor protein 1
AT3G11020:DRE/CRT-binding protein 2B
AT3G06160:AP2/B3-like transcriptional factor family protein
AT3G05800:AtBS1-interacting factor 1
AT4G34400:AP2/B3-like transcriptional factor family protein
AT5G10140:AGAMOUS-LIKE 25
AT5G24470:pseudo-response regulator 5
AT3G58120:BZIP61
AT2G42380:BZIP34
AT5G25830:GATA transcription factor 12
AT5G39860:PRE1 (PACLOBUTRAZOL RESISTANCE1)
AT2G21650:ARABIDOPSIS RAD-LIKE 2, MATERNAL EFFECT EMBRYO ARREST 3, RADIALIS-LIKE SANT/MYB 1, RSM1
AT1G68520:B-BOX DOMAIN PROTEIN 14
AT1G68840:RELATED TO ABI3/VP1 2 (RAV2)
AT1G78870:B-BOX DOMAIN PROTEIN 16, CONSTANS-LIKE 7
AT2G32550:Rcd1-like protein
AT3G06120:MUTE
AT2G36080:AP2/B3-like transcriptional factor family protein
AT4G09820:BHLH42, TRANSPARENT TESTA 8
AT1G13400:JAGGED-LIKE, NUBBIN
AT2G30420:ENHANCER OF TRY AND CPC 2, ETC2
AT1G04250:IAA17
AT1G70000:myb-like transcription factor family protein
AT3G22760:Tesmin/TSO1-like CXC domain-containing protein
AT3G63140:chloroplast stem-loop binding protein of 41 kDa
AT3G17609:HY5-homolog
AT1G71030:MYB-like 2
AT2G46680:homeobox 7
AT3G61890:homeobox 12
AT5G17300:Homeodomain-like superfamily protein
AT1G01060:Homeodomain-like superfamily protein
AT5G49330:myb domain protein 111
AT5G50915:basic helix-loop-helix (bHLH) DNA-binding superfamily protein
AT5G56840:myb-like transcription factor family protein

Supplemental Figure S13. Heat maps representing the fold change of DE genes in *GA20ox1* OE lines. Differentially expressed genes involved in secondary metabolism (A, F), protein synthesis (B, G), regulation of transcription (C, H), hormone metabolism (D), and photosynthesis (E) are shown. In (A, B, C), the average fold change of the transgenics per accession is represented and in (D, E, F, G, H), the fold change for each individual transgenic is shown. Names of genes are shown on the right side of the heat map and sample names are indicated on the top of heat map. Yellow and blue colours correspond to increased and decreased expression, respectively, in comparison with the wild types. Only DE genes that show at least a 1.5-fold change difference are shown. Hierarchical clustering was done for both genes and samples with Manhattan distance metrics.

A

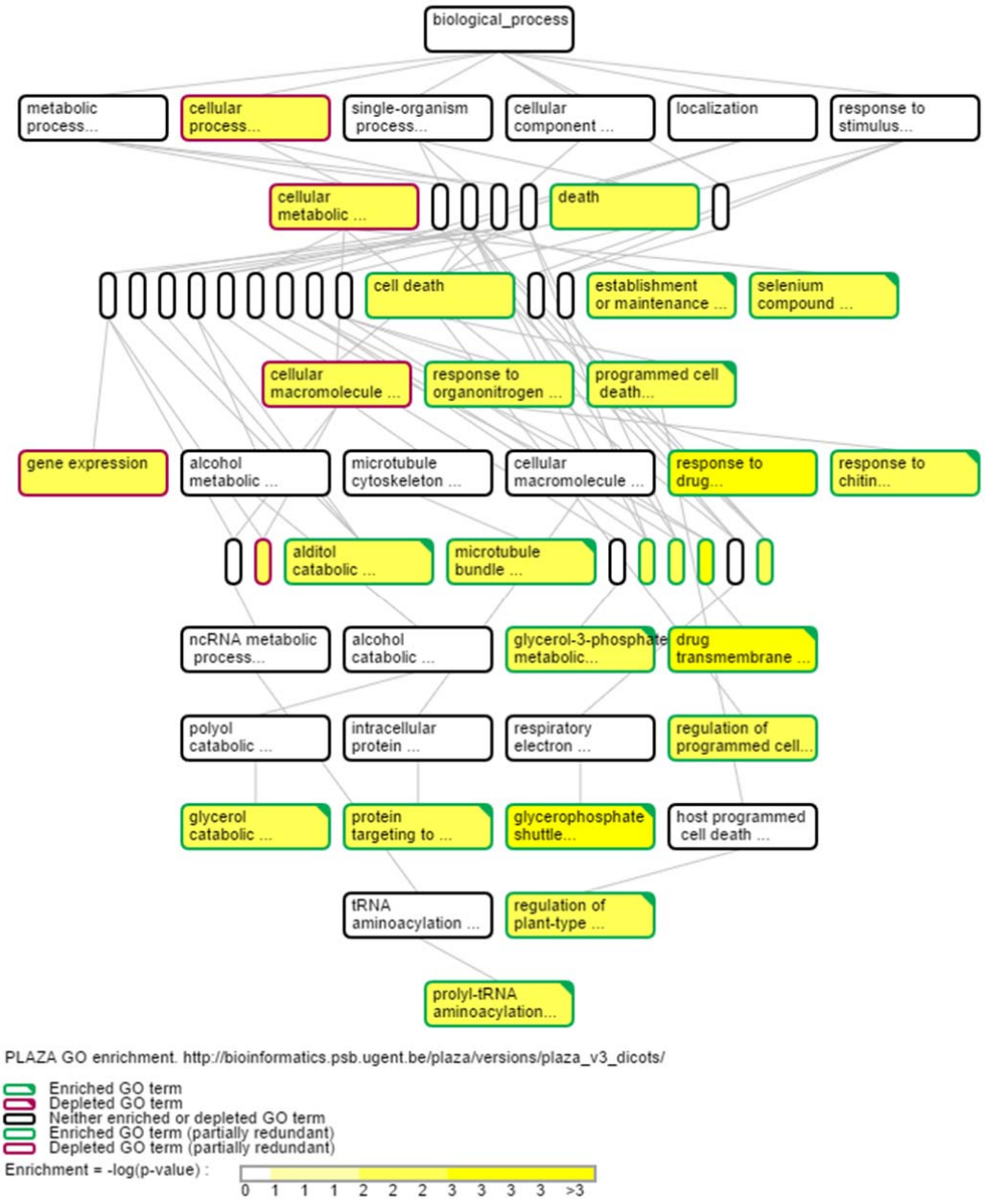
biological_process
metabolic process...
cellular process...
single-organism process...
cellular component ...
localization
response to stimulus...
cellular metabolic ...
death
cell death
establishment or maintenance ...
selenium compound ...
cellular macromolecule ...
response to organonitrogen ...
programmed cell death...
gene expression
alcohol metabolic ...
microtubule cytoskeleton ...
cellular macromolecule ...
response to drug...
response to chitin...
alditol catabolic ...
microtubule bundle ...
ncRNA metabolic process...
alcohol catabolic ...
glycerol-3-phosphate metabolic...
drug transmembrane ...
polyol catabolic ...
intracellular protein ...
respiratory electron ...
regulation of programmed cell...
glycerol catabolic ...
protein targeting to ...
glycerophosphate shuttle...
host programmed cell death ...
tRNA aminoacylation ...
regulation of plant-type ...
prolyl-tRNA aminoacylation...
PLAZA GO enrichment. http://bioinformatics.psb.ugent.be/plaza/versions/plaza_v3_dicots/
Enriched GO term
Depleted GO term
Neither enriched or depleted GO term
Enriched GO term (partially redundant)
Depleted GO term (partially redundant)
Enrichment = -log(p-value) :
0 1 1 1 2 2 2 3 3 3 3 >3

B

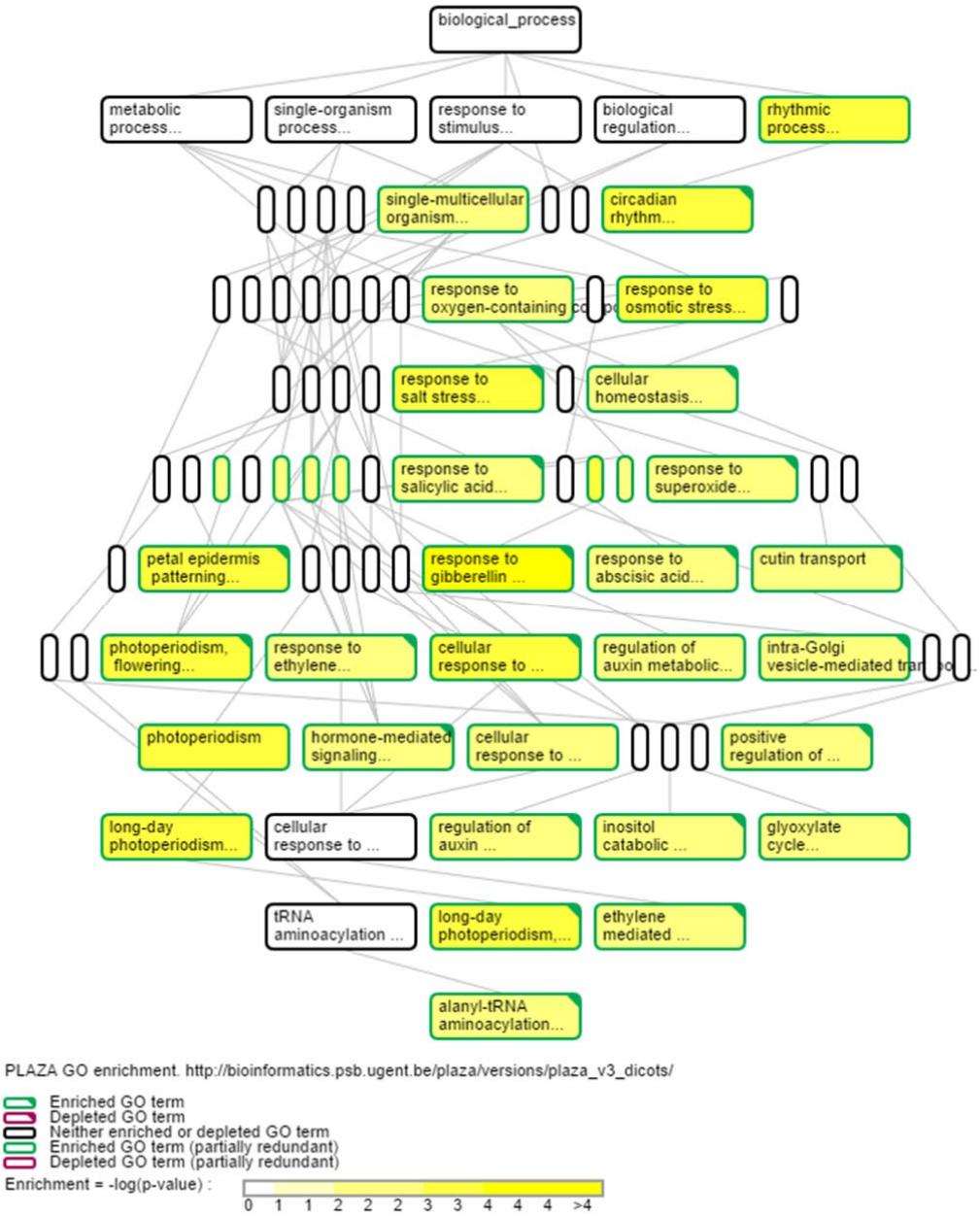

Supplemental Figure S14. Overrepresented GO categories (biological process) for genes positively (A) and negatively (B) correlated with rosette expressivity. GO enrichement analysis was performef using PLAZA (http://bioinformatics.psb.ugent.be/plaza/versions/plaza_v3_dicots/).

Supplemental Table S1. Geographic origin of the 17 Arabidopsis accessions used in this study.

Accession	Origin	CS stock number
An-1	Belgium	CS76091
Blh-1	Czech Republic	CS76098
C24	Portugal	CS76106
Col-0	Poland	CS76113
Cvi-0	Cape Verdi	CS76116
Ey15-2	Germany	CS76399
ICE138	Central Asia	CS76426
ICE153	Central Asia	CS76381
ICE163	Southern Tyrol	CS76353
ICE61	Russia	CS76378
ICE75	Russia	CS76422
ICE97	Southern Italy	CS76359
Ler-0	Germany	CS77020
Oy-0	Norway	CS76203
Sha	Tadjikistan	CS76382
WalhaesB4	Germany	CS76408
Yeg-1	Kaukasus	CS76394

Supplemental Table S3. Correlation between levels of different hormones in the 17 Arabidopsis accessions. Pearson correlations between 36 biosynthetic and degradation intermediates, and bioactive forms of six different hormones (GA, auxin, cytokinins, JA, SA and ABA) were calculated. Red colour indicates positive correlation. (Correlation coefficient > 0.6, adj-P value < 0.05) tZ, *trans*-zeatin; tZR, tZ riboside; tZRPs, tZR phosphates; cZ, *cis*-zeatin; cZR, cZ riboside; cZRPs, cZR phosphates; DZ, dihydrozeatin; DZR, DZ riboside; DZRPs, DZR phosphates; iP, N^6-(Δ^2-isopentenyl)adenine; iPR, iP riboside; iPRPs, iPR phosphates; tZ7G, tZ-7-*N*-glucoside; tZ9G, tZ-9-*N*-glucoside; tZOG, tZ-*O*-glucoside; tZROG, tZ-R-*O*-glucoside; cZROG, cZ-R-*O*-glucoside; tZRPsOG, tZR phosphates-*O*-glucoside; cZRPsOG, cZR phosphate-*O*-glucoside; DZ9G, DZ-9-*N*-glucoside; iP7G, iP-7-*N*-glucoside; iP9G, iP-9-*N*-glucoside; IAAsp, indole-3-acetyl aspartic acid; IAIle + IALeu, indole-3-acetyl-*L*-isoleusine + indole-3-acetyl-*L*-leucine; IAPhe, indole-3-acetyl-*L*-phenylalanine.

		Cytokinins																				GA							ABA	SA	JA	Auxin		
		tZ	tZR	tZRPs	cZ	cZR	cZRPs	DZ	DZR	DZRPs	iP	iPR	iPRPs	tZ7G	tZ9G	tZOG	tZROG	cZROG	tZRPsOG	cZRPsOG	DZ9G	iP7G	iP9G	GA_4	GA_8	GA_9	GA_{19}	GA_{24}	GA_{44}	GA_{53}				IAA	IAAsp	IAIle + IALeu	IAPhe
Cytokinins	tZ																																			
	tZR	0.58																																		
	tZRPs	0.41	0.25																																	
	cZ	0.38	0.55	-0.31																																
	cZR	-0.03	0.46	-0.47	0.78																															
	cZRPs	-0.06	0.38	-0.44	0.84	0.88																														
	DZ	0.45	0.11	0.15	0.36	0.21	0.16																													
	DZR	-0.10	0.40	-0.32	0.67	0.80	0.81	0.40																												
	DZRPs	0.03	-0.14	0.62	-0.19	-0.24	-0.15	0.56	0.15																											
	iP	0.71	0.52	0.18	0.49	0.20	0.16	0.23	-0.04	-0.12																										
	iPR	0.19	0.66	-0.31	0.74	0.91	0.76	0.15	0.65	-0.33	0.47																									
	iPRPs	0.16	0.18	0.43	-0.18	-0.09	-0.26	-0.07	-0.28	0.08	0.58	0.21																								
	tZ7G	0.76	0.37	0.61	-0.02	-0.36	-0.35	0.32	-0.31	0.31	0.47	-0.16	0.19																							
	tZ9G	0.76	0.33	0.57	0.00	-0.33	-0.32	0.38	-0.28	0.34	0.48	-0.14	0.17	0.99																						
	tZOG	0.43	-0.23	0.06	-0.17	-0.37	-0.44	0.27	-0.39	-0.01	0.09	-0.28	-0.03	0.40	0.45																					
	tZROG	0.54	0.49	0.85	-0.07	-0.23	-0.22	0.18	-0.13	0.50	0.33	-0.04	0.36	0.71	0.71	0.07																				
	cZROG	-0.35	-0.03	-0.16	-0.16	0.07	0.01	-0.53	-0.01	-0.18	0.06	0.17	0.37	-0.32	-0.37	-0.35	-0.24																			
	tZRPsOG	0.52	0.31	0.81	-0.08	-0.28	-0.25	0.25	-0.17	0.50	0.20	-0.17	0.19	0.65	0.66	0.19	0.94	-0.43																		
	cZRPsOG	-0.28	0.17	-0.18	0.18	0.34	0.38	-0.43	0.30	-0.10	0.17	0.38	0.23	-0.26	-0.30	-0.55	-0.10	0.84	-0.27																	
	DZ9G	0.18	-0.16	0.07	0.12	-0.04	0.05	0.80	0.28	0.65	-0.05	-0.17	-0.31	0.41	0.47	0.26	0.12	-0.49	0.20	-0.35																
	iP7G	0.33	0.07	0.04	0.06	-0.07	-0.17	0.10	-0.28	-0.07	0.60	0.15	0.56	0.51	0.51	0.37	0.10	0.08	-0.01	0.07	0.14															
	iP9G	0.31	0.14	-0.03	0.16	0.00	-0.08	0.05	-0.23	-0.19	0.58	0.20	0.48	0.45	0.43	0.35	0.03	0.04	-0.06	0.04	0.08	0.97														
GA	GA_4	0.42	0.29	0.59	0.03	-0.30	-0.19	-0.21	-0.37	0.07	0.23	-0.24	0.06	0.53	0.46	0.03	0.56	-0.20	0.55	-0.03	-0.19	0.17	0.21													
	GA_8	0.51	0.52	0.17	0.20	-0.07	-0.04	-0.12	-0.23	-0.22	0.61	0.12	0.18	0.65	0.61	-0.12	0.36	-0.09	0.21	0.09	-0.01	0.49	0.50	0.53												
	GA_9	0.62	0.50	0.53	0.30	-0.11	0.01	0.05	-0.12	0.10	0.46	0.00	0.05	0.62	0.62	0.02	0.71	-0.42	0.73	-0.11	0.02	0.14	0.16	0.80	0.64											
	GA_{19}	0.53	0.48	0.27	0.36	0.02	0.07	0.12	-0.07	0.02	0.70	0.18	0.30	0.63	0.62	-0.07	0.44	-0.24	0.36	0.06	0.13	0.60	0.62	0.58	0.86	0.77										
	GA_{24}	0.32	0.21	-0.09	0.16	-0.07	-0.08	-0.02	-0.18	-0.24	0.70	0.15	0.42	0.34	0.33	0.03	0.00	0.12	-0.13	0.20	0.01	0.65	0.66	0.12	0.71	0.27	0.70									
	GA_{44}	0.19	0.26	0.49	0.15	-0.01	0.13	0.08	0.07	0.31	0.00	-0.09	-0.11	0.19	0.22	-0.20	0.57	-0.54	0.63	-0.28	0.02	-0.28	-0.28	0.53	0.16	0.69	0.35	-0.29								
	GA_{53}	0.36	0.28	-0.05	0.20	-0.03	-0.06	0.05	-0.14	-0.22	0.74	0.19	0.50	0.30	0.31	0.01	0.02	0.02	-0.12	0.06	-0.03	0.66	0.66	0.10	0.66	0.28	0.74	0.89	-0.07							
ABA		0.73	0.56	0.37	0.38	0.10	0.05	0.37	0.05	0.11	0.45	0.20	-0.02	0.74	0.75	0.24	0.64	-0.50	0.69	-0.19	0.30	0.30	0.32	0.55	0.57	0.80	0.69	0.25	0.38	0.19						
SA		-0.33	-0.12	-0.38	0.49	0.53	0.77	0.18	0.64	0.10	-0.20	0.32	-0.41	-0.44	-0.39	-0.34	-0.30	-0.12	-0.24	0.18	0.27	-0.35	-0.31	-0.28	-0.33	-0.15	-0.22	-0.22	0.06	-0.33	-0.19					
JA		0.58	0.22	0.50	0.23	-0.02	0.01	0.49	0.00	0.47	0.38	0.01	0.09	0.63	0.69	0.22	0.69	-0.45	0.78	-0.22	0.45	0.22	0.13	0.36	0.26	0.65	0.49	-0.05	0.58	0.05	0.73	-0.12				
Auxin	IAA	0.63	0.44	0.01	0.42	0.26	0.18	0.21	-0.04	-0.18	0.89	0.51	0.48	0.47	0.49	0.13	0.21	0.13	0.09	0.22	0.05	0.66	0.61	0.04	0.58	0.25	0.57	0.60	-0.17	0.63	0.42	-0.24	0.39			
	IAAsp	0.59	0.30	0.04	0.36	0.30	0.17	0.35	0.01	-0.03	0.69	0.47	0.38	0.43	0.46	0.33	0.21	0.10	0.14	0.13	0.15	0.60	0.52	-0.03	0.25	0.09	0.30	0.24	-0.19	0.28	0.40	-0.19	0.49	0.88		
	IAIle + IALeu	0.61	0.36	-0.08	0.46	0.37	0.22	0.38	0.08	-0.12	0.63	0.49	0.21	0.45	0.46	0.35	0.11	0.02	0.06	0.07	0.21	0.60	0.56	-0.01	0.30	0.10	0.34	0.23	-0.21	0.27	0.47	-0.20	0.46	0.84	0.96	
	IAPhe	0.53	0.28	0.04	0.36	0.32	0.17	0.37	0.03	0.02	0.59	0.44	0.31	0.45	0.48	0.31	0.21	0.05	0.16	0.10	0.22	0.62	0.54	0.01	0.25	0.10	0.32	0.16	-0.13	0.22	0.44	-0.21	0.55	0.82	0.97	0.97

Supplemental Table S4. Percentage differences between the sequences of GA20ox1 in 15 accessions and Col-0 at DNA and protein level.

	GA20ox1	
Accession	**cDNA**	**Protein**
An-1	**0**	**0**
Blh-1	**0.09**	**0**
C24	**0.09**	**0**
Cvi-0	**0**	**0**
Ey15-2	**0.17**	**0**
ICE75	**0.17**	**0**
ICE97	**0.09**	**0**
ICE138	**0.09**	**0**
ICE153	**0**	**0**
ICE163	**0.09**	**0**
Ler-0	**0.17**	**0**
Oy-0	**0.09**	**0**
Sha	**0.17**	**0**
WalhaesB4	**0**	**0**
Yeg-1	**0**	**0**

Supplemental Table S9. Overrepresented MapMan categories for *GA20ox1* DE genes. The number of genes found in each overrepresented category is indicated. P-value with Bonferroni correction is shown.

Categories		Number of genes	P-value
Photosynthesis		46	5.14E-29
Secondary metabolism		47	3.98E-16
Protein		47	5.83E-11
Hormone metabolism		42	5.23E-10
RNA.regulation of transcription		92	
	RNA.regulation of transcription.C2C2(Zn) CO-like, Constans-like zinc finger family	8	1.33E-06
	RNA.regulation of transcription.MYB-related transcription factor family	8	3.60E-05
Transport		51	4.96E-05
Amino acid metabolism		19	8.55E-05
Sulfur-assimilation		3	
	Sulfur-assimilation.adenosine 5'-phosphosulfate reductase	3	2.02E-05